from macaques nasally immunized with PspA-nanogel were fully protected for at least 2 weeks (**Figure 3a,b**). In contrast, mice that received sera from macaques given nasal PspA alone or PBS only died within 5 days post-challenge (**Figure 3a,b**). These results demonstrated that protective immunity with subtype cross-reactivity was induced by nasal PspA-nanogel vaccination.

Nasal immunization with PspA-nanogel induces Th2 and Th17 responses in macaques

As macaques nasally immunized with PspA-nanogel showed high IgG/IgA Ab responses, we next determined the levels of cytokine production in CD4$^+$ T cells isolated from blood of the macaques. The macaques nasally immunized with PspA-nanogel showed increased levels of IL-4 and IL-17 production by CD4$^+$ T cells when compared with macaques given PspA alone or PBS only (**Figure 4b,c**). However, essentially identical levels of IFN-γ were produced by CD4$^+$ T cells isolated from macaques nasally immunized with PspA-nanogel, PspA alone, or PBS only (**Figure 4a**). Furthermore, we showed that nasal immunization with PspA-nanogel induced PspA-specific IgG1 Ab responses, which is the hallmark of the Th2-type immune response (**Figure 4d**). These results indicated that the nasal PspA-nanogel vaccine could induce Th2 and Th17 cytokine responses.
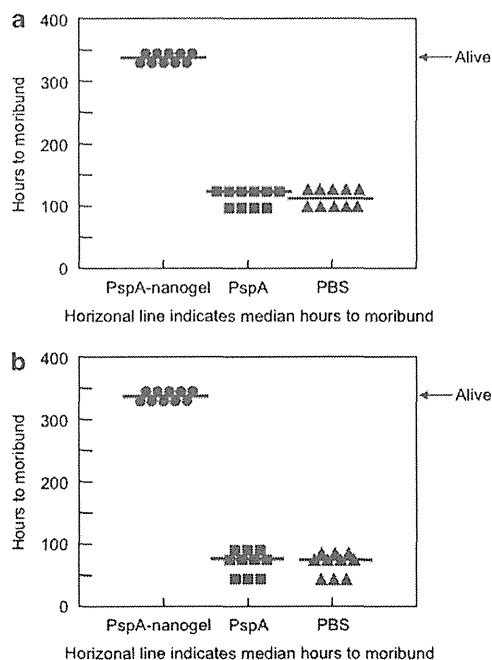
Figure 3 Neutralizing Abs induced by nasal immunization with PspA-nanogel. Serum from each of the macaques was collected 1 week after the final primary nasal immunization with PspA-nanogel, PspA alone, or PBS only. CBA/N mice (10 mice per group) were passively transferred with 100 μl of diluted (1:20) pooled sera via i.p. route. Four hours later, mice were injected i.v. with 1.5 × 10^4 c.f.u. *S. pneumoniae* Xen 10 (**a**) or 1 × 10^3 c.f.u. *S. pneumoniae* 3JYP2670 strain (**b**). The mice were monitored daily for mortality. Each line represents the median survival time. c.f.u., colony-forming unit; i.p., intraperitoneal; i.v., intravenous.

Nasal immunization with PspA-nanogel increases the expression levels of miRNAs in serum and respiratory tract tissues in macaques

To examine the roles of miRNA in the induction of PspA-specific immunity, we performed miRNA microarray analysis to identify immunologically associated differences in serum miRNA profiles between pre-immunized and post-boosted macaques (data not shown). We selected some immunologically relevant miRNAs, namely miR-181a, miR-326, miR-155, miR-17, miR-18a, miR-20a, and miR-92a, the levels of which were upregulated in post-booster serum samples compared with pre-immunized serum samples. To further confirm whether these immunologically relevant miRNAs were upregulated or downregulated in post-booster serum samples compared with pre-immunized or pre-booster serum samples, we performed quantitative RT–PCR of them. Expression levels of miR-326, Th17-cell differentiation-related miRNA, and miR-181a, T-cell and B-cell differentiation-related miRNA, were significantly increased in the sera of macaques given a nasal booster dose of PspA-nanogel when compared with control macaques as pre-immunization (**Figure 5a**). The levels of the two miRNAs were also shown significantly higher in the respiratory tract tissues, including nasal tissues and lungs, of macaques given a booster dose of PspA-nanogel than the levels in the corresponding tissues of control macaques given PspA alone or PBS only that was set at 1 (**Figure 5b,c**). Furthermore, we analyzed the expression level of Ets-1, which is a known negative regulator of Th17 cells and is the functional target of miR-326. We detected a significant decrease in the expression level of Ets-1 mRNA in the lungs of macaques given a booster dose of PspA-nanogel compared with those of control macaques given PspA alone or PBS only (**Figure 5c**). These results suggest that these miRNAs have important roles in T-cell and B-cell differentiation and in Th17 cytokine responses after nasal immunization with PspA-nanogel in macaques.

DISCUSSION

By using a nonhuman primate system, we demonstrated that the nasal PspA-nanogel vaccine did not accumulate in the CNS and effectively induced both mucosal and systemic immunity associated with protection against pneumococcal infection. To our knowledge, this study is the first to report the safety and effectiveness of a nasal PspA vaccine in macaques; therefore, our results provide a concrete rationale for testing our nanogel-based PspA vaccine in humans.

The nanogel itself is non-immunogenic material, and a cancer-specific protein (e.g., Her 2) complexed with a neutral CHP nanogel produced by means of good manufacturing practices (GMP) has been used as an injectable cancer vaccine in clinical research.[28] In our previous study, nasal immunization with CHP-nanogel containing PspA induces effective antigen-specific immune responses in mice[21] but not in macaques (data not shown); therefore, in the present study, we developed a cCHP nanogel containing 20 amino groups per 100 glucose units to improve antigen delivery to the nasal
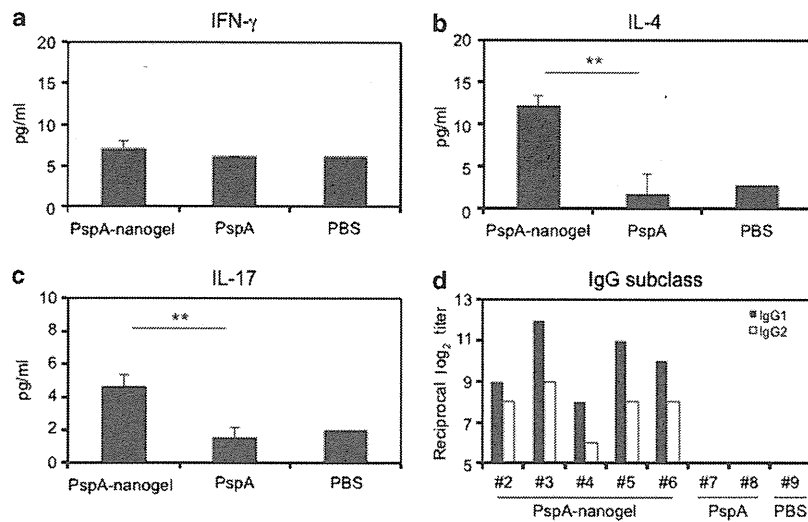
Figure 4 PspA-nanogel immunization produced CD4 + Th2- and Th17-type cytokine responses. CD4 + T cells were separated from the PBMCs 1 week after the booster. Purified CD4 + T cells were cultured with irradiated APCs and 5 μg ml $^{-1}$ of PspA with anti-CD28 and CD49d antibodies for 5 days. The levels of the cytokines, IFN-γ (a), IL-4 (b), and IL-17A (c) in the supernatants were measured. This experiment was repeated in triplicate. Values are shown as the means ± s.d. in each experimental group. **P< 0.01 compared between PspA-nanogel and PspA/PBS groups. (d) Serum from macaques was collected 1 week after the final primary nasal immunization with PspA-nanogel (#2–#6), PspA alone (#7, #8), or PBS only (#9). Expression levels of PspA-specific serum IgG subclass Abs were determined by using ELISA. APCs, antigen-presenting cells; IFN, interferon; IL, interleukin; PBMC, peripheral blood mononuclear cells.
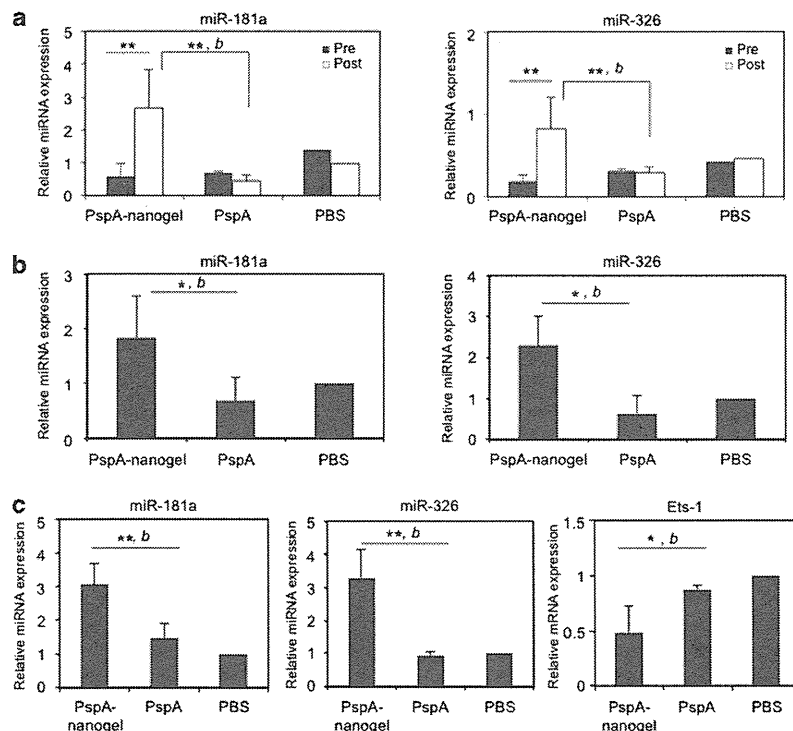

Figure 5 MiRNA expression levels in sera (a), nasal tissues (b), and lung tissues (c) of macaques nasally immunized with PspA-nanogel, PspA alone, or PBS only. Expression levels of the indicated miRNA and Ets-1 mRNA were analyzed by quantitative RT–PCR and normalized to the levels of miR-16 and β-actin, respectively. Values are shown as the means ± s.d. in each experimental group. *P < 0.05, **P < 0.01 when compared between pre-immunization and post-booster groups. b, Compared between PspA-nanogel and PspA/PBS groups in post-booster macaques. MiRNA, microRNA; Pre, pre-immunized serum; Post, post-booster serum.

epithelium layer of macaques. We confirmed the perfect complex formation and the size of PspA-nanogel complex using fluorescence response energy transfer (FRET) analysis and dynamic light scattering (DLS): the cCHP nanogel spontaneously formed nanoparticles after the incorporation of PspA (Supplementary Figure S1a,b).[18,19] In addition, consistent with its positive zeta-potential (Supplementary Figure S1b), in vivo PET and MRI imaging in macaques clearly showed that nasally administered cCHP nanogel carrying [18F]-labeled PspA was more effectively delivered to and continuously retained at the nasal mucosa of macaques when compared with nasally delivered [18F]-PspA alone. These results indicated that the new cationic group-modified cCHP nanogel would be able to efficiently deliver the vaccine antigen to the anionic nasal epithelium following nasal administration in macaques. Indeed, our previous mouse model studies have shown that the nanogel–antigen complex is retained and taken up into the epithelium by endocytosis, where the antigen is released from the nanogel in the epithelium by strong chaperone-like activity. The antigen is then released from the nasal epithelium by exocytosis and subsequently taken up effectively by DCs.[19,21]

Recent studies of nasal vaccines have raised concerns about the deposition and accumulation of candidate vaccine antigens or co-administered mucosal adjuvants in the CNS through direct transport from the nasal cavity to the cerebrum via the olfactory pathways.[29,30] It has also been reported that many peptides and proteins bypass the blood–brain and blood–cerebrospinal fluid barriers to reach the CNS following nasal administration in humans.[31] In this study, we showed that there was no deposition or accumulation of [18F]-PspA in the CNS over a period of up to 6 h after nasal administration of [18F]-PspA-nanogel in macaques. As we validated the detection limit of our PET system for [18F]-protein by direct tissue counting in our previous study,[32] [18F] radioactivity in this study was <0.05 SUV in the cerebrum and olfactory bulbs of the macaques. Therefore, our current results demonstrated that the cCHP delivered nasal PspA vaccine did not reach the CNS of macaques, even though the olfactory epithelium in the nasal cavity is connected to the CNS,[31] thereby confirming the safety of the vaccine in higher mammals.

The mucosal immune system consists of both inductive and effector sites and has a key role in the induction and regulation of dynamic immune responses, including the Th2-type-cell-dependent SIgA response, the mucosal cytotoxic T-cell response, and the Th17-cell-mediated immune regulatory response.[33] In general, IgA in mucosal tissue is thought to have an important role in protection against respiratory pathogens including S. pneumoniae.[15–17] In this study, we showed that the PspA-nanogel vaccine also induced mucosal antigen-specific mucosal IgA and systemic IgG Ab responses in the macaques. Especially, serum and BALF IgG, the main isotype of antibody in the lower respiratory compartment, have key roles in survival against lethal challenge with S. pneumoniae.[34] Importantly, the macaque IgG antibodies to PspA, which are supported by

CD4^{+} Th2-type cytokine IL-4, possessed protective activity against S. pneumoniae. When mice were systemically challenged with S. pneumoniae Xen10 or 3JYP2670 after mice passively immunized with macaques' sera containing PspA-specific Abs, they showed complete protection. Our findings indicate that this protection is clearly due to antibody-mediated immunity to PspA. These results are consistent with those of a previous study in mice showing that nasal vaccination induces functional CD4^{+} Th2-type cytokine-mediated IgG Ab responses, which are sufficient to provide appropriate protection in the absence of Th1-type cytokine responses.[16] In addition, induction of the BALF IgG responses is essential, as antigen-specific IgG is known to exert protection at the alveolar level following to promote phagocytosis and prevents local dissemination of the pneumococcus and its passage into the blood.[34] These results demonstrated that the nasal PspA-nanogel vaccine effectively induced PspA-specific serum IgG with protective activity in addition to SIgA Ab immune responses in nonhuman primates.

Recent studies have shown that specific miRNAs are involved in T-cell and B-cell development, differentiation, and regulatory functions.[24,35] Especially, miR-181a is highly expressed in mature T cells and has an important effect on the positive and negative selection process by controlling the strength of TCR signaling during thymic development of T cells for subsequent Th1 and Th2 differentiation, indicating that miR-181a modulates T-cell development.[36] In this study, the expression levels of miR-181a in the serum and respiratory tract tissues, including nasal tissues and lungs, were significantly higher in macaques nasally immunized with PspA-nanogel than in those given PspA alone or PBS only, indicating that miRNAs are implicated in adaptive immunity by controlling the activation of T cells after nasal immunization with PspA-nanogel in nonhuman primates. Furthermore, we showed that the levels of miR-155, which is required for the production of high-affinity IgG1 Abs, were increased in PspA-nanogel-immunized macaques (Supplementary Figure S2a–c).[37] These results indicated that PspA-nanogel-induced Th2 cytokine response was mediated through the increased expression of miR-155.

MiR-181a is also highly expressed in B cells and within bone marrow cells and germinal center B cells, where it promotes the differentiation of hematopoietic stem cells into B cells.[24,38] To explore the roles of other miRNAs that are also highly expressed in germinal center B cells and are essential for adult B-cell development, we examined the expression of the miR-17-92 cluster.[39,40] The miR-17-92 cluster regulates follicular helper T cell (Tfh cell) differentiation by controlling the migration of CD4^{+} T cells into B-cell follicles,[41] suggesting that these miRNAs have an important role in the production of antigen-specific SIgA Ab. We found here that not only miR-181a expression but also miR-17-92 cluster expression was markedly increased in the nasal tissues of nasally PspA-nanogel-immunized macaques (Supplementary Figure S3). Detection of these mucosal IgA-associated miRNAs in the nasal tissues of nasally PspA-nanogel-immunized macaques

indicates that they contribute substantially to the production of mucosal IgA.

It is well known that IL-17-mediated CD4$^+$ T cells are important for the generation of resistance to mucosal colonization by respiratory pathogens including S. pneumoniae in humans and mice.[42,43] Trzcinski et al.[44] demonstrated that antigen-specific CD4$^+$ T-cell immunity is sufficient to protect against nasopharyngeal colonization by S. pneumoniae in mice. Studies in mice indicated that pulmonary Th17 responses are associated with migration of B cells into airways and with the promotion of polymeric Ig receptor (pIgR) expression by airway epithelial cells.[45] In addition, Th17 cells are a crucial subset of Th cells responsible for inducing the switch of germinal center B cells toward T-cell-dependent IgA production.[46] Furthermore, IL-17-secreting memory Th17 cells increased by human pneumococcal carriage have been reported to enhance innate cellular immunity against pneumococcal challenge.[47] Therefore, it is important to determine whether antigen-specific CD4$^+$ Th17 responses are induced by nasal immunization with PspA-nanogel in nonhuman primates. Recent studies have shown that miR-326-mediated Th17 upregulation might provide the host with a potentiating effect to recruit functional immune cells to local effector sites in response to pathogen attack.[48] We found here that nasal immunization with PspA-nanogel in macaques prompted the generation of IL-17-producing cells in the peripheral blood CD4$^+$ T cells. Furthermore, our miRNA analysis showed that expression levels of Th17-associated miR-326 in the serum, nasal tissues, and lungs were significantly increased and that the expression level of Ets-1 mRNA, a negative regulator of Th17 differentiation, was decreased in the lungs of the PspA-nanogel-vaccinated macaques. Therefore, our finding that miR-326-associated IL-17-secreting CD4$^+$ T cells were generated after nasal vaccination with PspA-nanogel suggests that it would be useful for the development of safe and efficacious nasal vaccines against pneumonia and that serum miR-326 could be used as a biomarker to evaluate vaccine efficacy.

In summary, we demonstrated for the first time that a nasal PspA-nanogel vaccine induced both humoral and cellular immune responses in macaques. These results were supported by increased expression levels of miR-181a and miR-326, which are candidate miRNA biomarkers for induction of mucosal immunity. In addition, a [^{18}F]-PspA PET study showed long-term retention of PspA in the nasal cavity and no deposition of PspA in the CNS of the macaques. Taken together, these findings demonstrate the efficacy and safety of nasal PspA-nanogel vaccine in nonhuman primates. We conclude that the nasal PspA-nanogel vaccine should now be studied in humans for its possible use as an adjuvant-free nasal vaccine.

METHODS

Animals. Eight female naive cynomolgus macaques (Macaca fascicularis, 5 years old, ~3 kg) were used for the immunization study and were maintained at the Tsukuba Primate Research Center for Medical Science at the National Institute of Biomedical Innovation (NIBIO, Ibaraki, Japan). In a separate experiment, one naive male rhesus macaque (M. mulatta, 5–6 years old, ~5 kg) was used for the PET imaging study, which was conducted at PET Center of Hamamatsu Photonics K.K. To assay antibody protection against S. pneumoniae, female CBA/N mice (6 weeks old) were purchased from Japan SLC (Shizuoka, Japan). All experiments were performed in accordance with the Guidelines for Use and Care of Experimental Animals, and the protocol was approved by the Animal Committee of NIBIO, Hamamatsu Photonics K.K., and The University of Tokyo.

Recombinant PspA. Recombinant PspA of S. pneumoniae Rx1, which belongs to PspA family 1 and clade 2, was prepared as described previously, with slight modification.[10] In brief, the plasmid encoding PspA/Rx1 (GenBank accession no. M74122; amino acids 1 through 302, pUAB055) was used to transform E. coli BL21 (DE3) cells. To construct pUAB055, a 909-bp fragment of PspA from a pneumococcal strain Rx1 was cloned into the pET20b vector (Novagen, Darmstadt, Germany) between the NcoI and XhoI sites. Recombinant PspA/Rx1 contains the first 302 amino acids of mature PspA plus six poly-histidines added through protein fusion at the C-terminal end. The sonicated cell supernatant was loaded onto a DEAE-Sepharose column (BD Healthcare, Piscataway, NJ) and a nickel affinity column (Qiagen, Valencia, CA), followed by gel filtration on a Sephadex G-100 column (BD Healthcare).

Preparation of recombinant PspA–nanogel complex. The cCHP nanogel (~40 nm size) generated from cationic type of cholesteryl group-bearing pullulan was used for all experiments. This cCHP nanogel contained 20 amino groups per 100 glucose units. The PspA-cCHP nanogel complex for each immunization was prepared by mixing 25 μg of PspA with cCHP at a 1:5 molecular ratio (59.45 μl per macaque) and incubating for 1 h at 46 °C. FRET was determined with an FP-6500 fluorescence spectrometer (JASCO, Tokyo, Japan) with FITC-conjugated PspA and TRITC-conjugated cCHP nanogel.[18,19] The hydrodynamic radius was assessed by means of DLS and the zeta-potential of cCHP carrying or not carrying, PspA was determined with a Zetasizer Nano ZS instrument (Malvern Instruments, Worcestershire, UK).[18,19]

Nasal immunization and sample collection. Cynomolgus macaques were nasally immunized five times at 2-week intervals with PspA-nanogel under ketamine anesthesia. For the control group, macaques were nasally administered with 25 μg of PspA alone, or PBS only. Eight months after the final immunization, the macaques were nasally boosted with the same amount of PspA-nanogel, PspA alone or PBS only. Serum, nasal wash, and BALF were collected before primary immunization, 1 week after each immunization, 2, 4, 6, and 8 months after the final immunization, and 2 weeks after receipt of the booster.

PspA-specific ELISA. The antigen-specific Ab responses were analyzed by ELISA as described previously.[21] In brief, 96-well plates were coated with 1 μg ml^{-1} PspA in PBS overnight at 4 °C. After blocking with 1 % BSA in PBS-Tween, twofold serial dilutions of samples were added and incubated for 2 h at room temperature (RT). After washing of the samples, horseradish peroxidise (HRP)-conjugated goat anti-monkey IgG (Nordic Immunological Laboratory, Tilburg, The Netherlands) or HRP-conjugated goat anti-monkey IgA (Cortex Biochem, San Leandro, CA) diluted 1:1,000 was added and incubated for 2 h at room temperature. For subclass analysis, sheep anti-human IgG1 and IgG2 (Binding Site, Birmingham, UK) and HRP-conjugated donkey anti-sheep IgG (Rockland, Limerick, PA) were used for detection. The reaction was developed with the use of TMB Microwell Peroxidase Substrate System (XPL, Gaithersburg, MD). End-point titers were expressed as the reciprocal log$_2$ of the last dilution that gave an OD$_{450}$ of 0.1 greater than the negative control.

Passive protection of mice with macaques' serum samples. Pooled serum samples from macaques nasally immunized with PspA-

nanogel, PspA alone, or PBS only were diluted with PBS (1:20) and injected into CBA/N mice via the intraperitoneal route (100 μl per mouse). Four hours later, all groups of mice were challenged with 1.5×10^4 CFU *S. pneumoniae* Xen 10 ($LD_{50} = 2 \times 10^2$ CFU for CBA/N mice) or 1×10^3 CFU *S. pneumoniae* 3JYP2670 strain ($LD_{50} = 7 \times 10^2$ CFU for CBA/N mice) via the intravenous route and observed daily for death for 2 weeks. Information about *S. pneumoniae* strains is available in **Supplementary Materials**.

PspA-specific CD4$^+$ T-cell responses. One week after the macaques had received the booster, lymphocytes were isolated from the peripheral blood by using Ficoll-Paque PLUS (GE Healthcare, Little Chalfont, UK). We could not separate the lymphocytes from two macaques (#3 and #6). After washing of the samples, CD4$^+$ T cells were purified by using CD4 microbeads and magnetic cell sorting (AutoMACS; Miltenyi Biotec, Auburn, CA). The cells remaining after the removal of CD4$^+$ and CD8$^+$ T cells (by using CD8 microbeads) were used as antigen-presenting cells after irradiation at 3,000 rad. Purified CD4$^+$ T cells (1×10^5 cells/well) and antigen-presenting cells (0.5×10^5 cells/well) were resuspended in RPMI 1640 (Nacalai Tesque, Kyoto, Japan) supplemented with 10 % FCS and penicillin-streptomycin (Gibco, Carlsbad, CA), and were cultured in 24-well plates for 5 days in the presence of $5\,\mu g\,ml^{-1}$ PspA with anti-CD28 (clone CD28.2) and CD49d (clone 9F10) antibodies ($0.5\,\mu g\,ml^{-1}$ each; eBioscience, San Diego, CA) at 37 °C in 5% CO_2. Supernatants were then collected. The concentrations of the cytokines, IFN-γ, IL-4, and IL-17 in the supernatants were measured with a Monkey Singleplex Bead Kit (Invitrogen, Carlsbad, CA) and Bio-Plex 200 (Bio-Rad, Hercules, CA).

Synthesis of [^{18}F]-PspA. Purified PspA was radiolabeled by conjugation with *N*-succinimidyl-4-[^{18}F]fluorobenzoate ([^{18}F]SFB), which reacts with free amino groups, including the N-terminal and ε-Lys amino groups in the protein, as described previously.[19,32] The product was purified by gel-permeation chromatography (Superose 12, PBS, 1 ml min^{-1}), and the radioactive peak that eluted at 12.7 min was collected. The 615 MBq [^{18}F]-PspA was obtained at 150 min from the end of bombardment. The radiochemical purity and the decay-corrected radiochemical yield were 100 and 2.95%, respectively. The specific activity was 1,798 to 4,045 MBq mg^{-1} protein.

PET/MRI imaging in rhesus macaques. Because the half-life of [^{18}F] is only 110 min, we used the same naive macaque for nasal [^{18}F]-PspA-nanogel or [^{18}F]-PspA-PBS administration with a 1-week interval between administrations. After nasal administration of 50 MBq per 700 μl of [^{18}F]-PspA-nanogel or [^{18}F]-PspA-PBS (350 μl in each nostril), the macaque's head was tilted back for 10 min and then scanned in an upright position. PET scans were conducted for 345 min with frames of 25×3 min, followed by 27×10 min, with the use of a high-resolution animal PET scanner (SHR-7700; Hamamatsu Photonics, Shizuoka, Japan). MRI images were recorded with Signa Excite HDxt (3T; GE Healthcare) to identify the cerebrum regions.

Image data analysis. PET data were analyzed by means of the PMOD software package (PMOD Technologies, Zurich, Switzerland). Each PET image was superimposed on the corresponding MRI data to identify the volume of interest. Time-activity curves (TACs) of PET/MRI images were expressed as % remaining dose.

MiRNA expression levels in serum and respiratory tract tissues. Serum samples were collected before primary immunization and after booster with PspA-nanogel, PspA alone, or PBS only. The respiratory tract tissues, which included nasal epithelial and lung samples, were collected after booster immunization with PspA-nanogel, PspA alone, or PBS only. Total RNAs were isolated from serum by using TRIzol LS reagent, and from nasal tissue or lung by using TRIzol reagent (Invitrogen) following the manufacturer's protocol. All the miRNAs in the sample were polyadenylated by using poly(A) polymerase and ATP (Invitrogen). Following polyadenylation, SuperScript III RT and a specially designed Universal RT Primer (Invitrogen) were used to

synthesize cDNA from the tailed miRNA population. Each of the first-strand cDNAs was analyzed by quantitative RT-PCR with Fast SYBR Green Master Mix and Step One Plus Real-Time PCR System (Applied Biosystems, Carlsbad, CA). The expression levels were normalized to miR-16, which is a commonly used internal control for miRNA expression.[49,50]

Analysis of Ets-1 expression. After total RNAs were isolated from lung tissue, cDNA was synthesized by using PrimeScript RT Master Mix (Takara, Shiga, Japan) following the manufacturer's protocol. The cDNA was analyzed by quantitative RT-PCR with Fast SYBR Green Master Mix and Step One Plus Real-Time PCR System (Applied Biosystems). The PCR primers were used as follows: Ets-1: F, 5′-TGG AGTCAACCCAGCCTATC-3′ and R, 5′-TCTGCAAGGTGTCTGTC TGG-3′; β-actin: F, 5′-TGACGTGGACATCCGCAAAG-3′ and R, 5′-CTGGAAGGTGGACAGCGAGG-3′. The expression levels were normalized to that of β-actin.

Statistical analysis. The results are presented as means ± s.d. Student's *t*-test was used for comparisons among groups. The *P* values <0.05 or <0.01 were considered to indicate statistical significance.

SUPPLEMENTARY MATERIAL is linked to the online version of the paper at http://www.nature.com/mi

REFERENCES
1. Jackson, L.A. & Janoff, E.N. Pneumococcal vaccination of elderly adults: new paradigms for protection. *Clin. Infect. Dis.* **47**, 1328–1338 (2008).
2. Nuorti, J.P. & Whitney, C.G. Prevention of pneumococcal disease among infants and children - use of 13-valent pneumococcal conjugate vaccine and 23-valent pneumococcal polysaccharide vaccine - recommendations of the Advisory Committee on Immunization Practices (ACIP). *MMWR Recomm. Rep.* **59**, 1–18 (2010).
3. Oosterhuis-Kafeja, F., Beutels, P. & Van Damme, P. Immunogenicity, efficacy, safety and effectiveness of pneumococcal conjugate vaccines (1998-2006). *Vaccine* **25**, 2194–2212 (2007).
4. Dagan, R. *et al.* Reduction of nasopharyngeal carriage of Streptococcus pneumoniae after administration of a 9-valent pneumococcal conjugate vaccine to toddlers attending day care centers. *J. Infect. Dis.* **185**, 927–936 (2002).
5. Dagan, R. *et al.* Comparative immunogenicity and efficacy of 13-valent and 7-valent pneumococcal conjugate vaccines in reducing nasopharyngeal colonization: a randomized double-blind trial. *Clin. Infect. Dis.* **57**, 952–962 (2013).
6. Croney, C.M., Coats, M.T., Nahm, M.H., Briles, D.E. & Crain, M.J. PspA family distribution, unlike capsular serotype, remains unaltered following introduction of the heptavalent pneumococcal conjugate vaccine. *Clin. Vaccine Immunol.* **19**, 891–896 (2012).
7. Pilishvili, T. *et al.* Sustained reductions in invasive pneumococcal disease in the era of conjugate vaccine. *J. Infect. Dis.* **201**, 32–41 (2010).

8. Berry, A.M., Yother, J., Briles, D.E., Hansman, D. & Paton, J.C. Reduced virulence of a defined pneumolysin-negative mutant of *Streptococcus pneumoniae*. *Infect. Immun.* **57**, 2037–2042 (1989).

9. McDaniel, L.S. *et al.* Use of insertional inactivation to facilitate studies of biological properties of pneumococcal surface protein A (PspA). *J. Exp. Med.* **165**, 381–394 (1987).

10. Briles, D.E. *et al.* Intranasal immunization of mice with a mixture of the pneumococcal proteins PsaA and PspA is highly protective against nasopharyngeal carriage of *Streptococcus pneumoniae*. *Infect. Immun.* **68**, 796–800 (2000).

11. Nguyen, C.T., Kim, S.Y., Kim, M.S., Lee, S.E. & Rhee, J.H. Intranasal immunization with recombinant PspA fused with a flagellin enhances cross-protective immunity against *Streptococcus pneumoniae* infection in mice. *Vaccine* **29**, 5731–5739 (2011).

12. McCool, T.L., Cate, T.R., Moy, G. & Weiser, J.N. The immune response to pneumococcal proteins during experimental human carriage. *J. Exp. Med.* **195**, 359–365 (2002).

13. Kono, M., Hotomi, M., Hollingshead, S.K., Briles, D.E. & Yamanaka, N. Maternal immunization with pneumococcal surface protein A protects against pneumococcal infections among derived offspring. *PLoS One* **6**, e27102 (2011).

14. Fukuyama, Y. *et al.* A combination of Flt3 ligand cDNA and CpG oligodeoxynucleotide as nasal adjuvant elicits protective secretory-IgA immunity to *Streptococcus pneumoniae* in aged mice. *J. Immunol.* **186**, 2454–2461 (2011).

15. Ferreira, D.M. *et al.* Characterization of protective mucosal and systemic immune responses elicited by pneumococcal surface protein PspA and PspC nasal vaccines against a respiratory pneumococcal challenge in mice. *Clin. Vaccine Immunol.* **16**, 636–645 (2009).

16. Fukuyama, Y. *et al.* Secretory-IgA antibodies play an important role in the immunity to *Streptococcus pneumoniae*. *J. Immunol.* **185**, 1755–1762 (2010).

17. Janoff, E.N. *et al.* Killing of *Streptococcus pneumoniae* by capsular polysaccharide-specific polymeric IgA, complement, and phagocytes. *J. Clin. Invest.* **104**, 1139–1147 (1999).

18. Ayame, H., Morimoto, N. & Akiyoshi, K. Self-assembled cationic nanogels for intracellular protein delivery. *Bioconjug. Chem.* **19**, 882–890 (2008).

19. Nochi, T. *et al.* Nanogel antigenic protein-delivery system for adjuvant-free intranasal vaccines. *Nat. Mater.* **9**, 572–578 (2010).

20. Yuki, Y. *et al.* Nanogel-based antigen-delivery system for nasal vaccines. *Biotechnol. Genet. Eng. Rev.* **29**, 61–72 (2013).

21. Kong, I.G. *et al.* Nanogel-based PspA intranasal vaccine prevents invasive disease and nasal colonization by *Streptococcus pneumoniae*. *Infect. Immun.* **81**, 1625–1634 (2013).

22. Baltimore, D., Boldin, M.P., O'Connell, R.M., Rao, D.S. & Taganov, K.D. MicroRNAs: new regulators of immune cell development and function. *Nat. Immunol.* **9**, 839–845 (2008).

23. O'Connell, R.M., Rao, D.S., Chaudhuri, A.A. & Baltimore, D. Physiological and pathological roles for microRNAs in the immune system. *Nat. Rev. Immunol.* **10**, 111–122 (2010).

24. Zhu, S., Pan, W. & Qian, Y. MicroRNA in immunity and autoimmunity. *J. Mol. Med.* **91**, 1039–1050 (2013).

25. Cobb, B.S. *et al.* T cell lineage choice and differentiation in the absence of the RNase III enzyme Dicer. *J. Exp. Med.* **201**, 1367–1373 (2005).

26. Muljo, S.A. *et al.* Aberrant T cell differentiation in the absence of Dicer. *J. Exp. Med.* **202**, 261–269 (2005).

27. Koralov, S.B. *et al.* Dicer ablation affects antibody diversity and cell survival in the B lymphocyte lineage. *Cell* **132**, 860–874 (2008).

28. Kitano, S. *et al.* HER2-specific T-cell immune responses in patients vaccinated with truncated HER2 protein complexed with nanogels of cholesteryl pullulan. *Clin. Cancer Res.* **12**, 7397–7405 (2006).

29. van Ginkel, F.W., Jackson, R.J., Yuki, Y. & McGhee, J.R. Cutting edge: the mucosal adjuvant cholera toxin redirects vaccine proteins into olfactory tissues. *J. Immunol.* **165**, 4778–4782 (2000).

30. Yuki, Y. & Kiyono, H. Mucosal vaccines: novel advances in technology and delivery. *Expert Rev. Vaccines* **8**, 1083–1097 (2009).

31. Illum, L. Is nose-to-brain transport of drugs in man a reality? *J. Pharm. Pharmacol.* **56**, 3–17 (2004).

32. Yuki, Y. *et al.* In vivo molecular imaging analysis of a nasal vaccine that induces protective immunity against botulism in nonhuman primates. *J. Immunol.* **185**, 5436–5443 (2010).

33. Fukuyama, Y. *et al.* Novel vaccine development strategies for inducing mucosal immunity. *Expert Rev. Vaccines* **11**, 367–379 (2012).

34. Twigg, H.L. 3rd Humoral immune defense (antibodies): recent advances. *Proc. Am. Thorac. Soc.* **2**, 417–421 (2005).

35. Baumjohann, D. & Ansel, K.M. MicroRNA-mediated regulation of T helper cell differentiation and plasticity. *Nat. Rev. Immunol.* **13**, 666–678 (2013).

36. Li, Q.J. *et al.* miR-181a is an intrinsic modulator of T cell sensitivity and selection. *Cell* **129**, 147–161 (2007).

37. Vigorito, E. *et al.* microRNA-155 regulates the generation of immunoglobulin class-switched plasma cells. *Immunity* **27**, 847–859 (2007).

38. Chen, C.Z., Li, L., Lodish, H.F. & Bartel, D.P. MicroRNAs modulate hematopoietic lineage differentiation. *Science* **303**, 83–86 (2004).

39. Tan, L.P. *et al.* miRNA profiling of B-cell subsets: specific miRNA profile for germinal center B cells with variation between centroblasts and centrocytes. *Lab. Invest.* **89**, 708–716 (2009).

40. Ventura, A. *et al.* Targeted deletion reveals essential and overlapping functions of the miR-17 through 92 family of miRNA clusters. *Cell* **132**, 875–886 (2008).

41. Kang, S.G. *et al.* MicroRNAs of the miR-17-92 family are critical regulators of T(FH) differentiation. *Nat. Immunol.* **14**, 849–857 (2013).

42. Lu, Y.J. *et al.* Interleukin-17A mediates acquired immunity to pneumococcal colonization. *PLoS Pathog.* **4**, e1000159 (2008).

43. Malley, R. *et al.* $CD4^+$ T cells mediate antibody-independent acquired immunity to pneumococcal colonization. *Proc. Natl. Acad. Sci. USA* **102**, 4848–4853 (2005).

44. Trzcinski, K. *et al.* Protection against nasopharyngeal colonization by *Streptococcus pneumoniae* is mediated by antigen-specific $CD4^+$ T cells. *Infect. Immun.* **76**, 2678–2684 (2008).

45. Jaffar, Z., Ferrini, M.E., Herritt, L.A. & Roberts, K. Cutting edge: lung mucosal Th17-mediated responses induce polymeric Ig receptor expression by the airway epithelium and elevate secretory IgA levels. *J. Immunol.* **182**, 4507–4511 (2009).

46. Hirota, K. *et al.* Plasticity of Th17 cells in Peyer's patches is responsible for the induction of T cell-dependent IgA responses. *Nat. Immunol.* **14**, 372–379 (2013).

47. Wright, A.K. *et al.* Experimental human pneumococcal carriage augments IL-17A-dependent T-cell defence of the lung. *PLoS Pathog.* **9**, e1003274 (2013).

48. Du, C. *et al.* MicroRNA miR-326 regulates TH-17 differentiation and is associated with the pathogenesis of multiple sclerosis. *Nat. Immunol.* **10**, 1252–1259 (2009).

49. Chang, K.H., Mestdagh, P., Vandesompele, J., Kerin, M.J. & Miller, N. MicroRNA expression profiling to identify and validate reference genes for relative quantification in colorectal cancer. *BMC Cancer* **10**, 173 (2010).

50. Mizuno, H. *et al.* Identification of muscle-specific microRNAs in serum of muscular dystrophy animal models: promising novel blood-based markers for muscular dystrophy. *PLoS One* **6**, e18388 (2011).
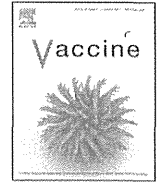
Recombinant Ag85B vaccine by taking advantage of characteristics of human parainfluenza type 2 virus vector showed Mycobacteria-specific immune responses by intranasal immunization

Kenta Watanabe[a,1], Akihiro Matsubara[a,b,1], Mitsuo Kawano[c], Satoru Mizuno[d,e],
Tomotaka Okamura[a], Yusuke Tsujimura[a], Hiroyasu Inada[f], Tetsuya Nosaka[c],
Kazuhiro Matsuo[d], Yasuhiro Yasutomi[a,b,*]

[a] Laboratory of Immunoregulation and Vaccine Research, Tsukuba Primate Research Center, National Institute of Biomedical Innovation, Tsukuba, Ibaraki 305-0843, Japan
[b] Division of Immunoregulation, Department of Molecular and Experimental Medicine, Mie University Graduate School of Medicine, Tsu, Mie 514-8507, Japan
[c] Department of Microbiology and Molecular Genetics, Mie University Graduate School of Medicine, Tsu, Mie 514-8507, Japan
[d] Research and Development Department, Japan BCG Laboratory, Kiyose, Tokyo 204-0022, Japan
[e] The Research Institute of Tuberculosis, Kiyose, Tokyo 204-8533, Japan
[f] Department of Pathology, Faculty of Pharmaceutical Science, Suzuka University of Medical Science, Suzuka, Mie 513-8670, Japan

ARTICLE INFO

ABSTRACT

Viral vectors are promising vaccine candidates for eliciting suitable Ag-specific immune response. Since Mycobacterium tuberculosis (Mtb) normally enters hosts via the mucosal surface of the lung, the best defense against Mtb is mucosal vaccines that are capable of inducing both systemic and mucosal immunity. Although Mycobacterium bovis bacille Calmette-Guérin is the only licensed tuberculosis (TB) vaccine, its efficacy against adult pulmonary forms of TB is variable. In this study, we assessed the effectiveness of a novel mucosal TB vaccine using recombinant human parainfluenza type 2 virus (rhPIV2) as a vaccine vector in BALB/c mice. Replication-incompetent rhPIV2 (M gene-eliminated) expressing Ag85B (rhPIV2–Ag85B) was constructed by reverse genetics technology. Intranasal administration of rhPIV2–Ag85B induced Mtb-specific immune responses, and the vaccinated mice showed a substantial reduction in the number of CFU of Mtb in lungs and spleens. Unlike other viral vaccine vectors, the immune responses against Ag85B induced by rhPIV2–Ag85B immunization had an advantage over that against the viral vector. In addition, it was revealed that rhPIV2–Ag85B in itself has an adjuvant activity through the retinoic acid-inducible gene I receptor. These findings provide further evidence for the possibility of rhPIV2–Ag85B as a novel TB vaccine.

1. Introduction

Recombinant viral vector vaccines have several advantages for preventing infection with pathogens [1]. The vaccines induce a full spectrum of immune responses including humoral and cellular immune responses. These immune responses can be initially induced at the viral vector infection site such as mucosal immune responses [2]. Moreover, the viral vector itself has adjuvant activities through the innate immune systems [3]. Pre-existing or post-priming immune responses against the vaccine vector itself, however, could be an obstacle to effective immune responses to recombinant Ag [4]. Negligible immune responses against vector viruses compared with recombinant vaccine Ags after immunization is considered most desirable for recombinant viral vaccines.
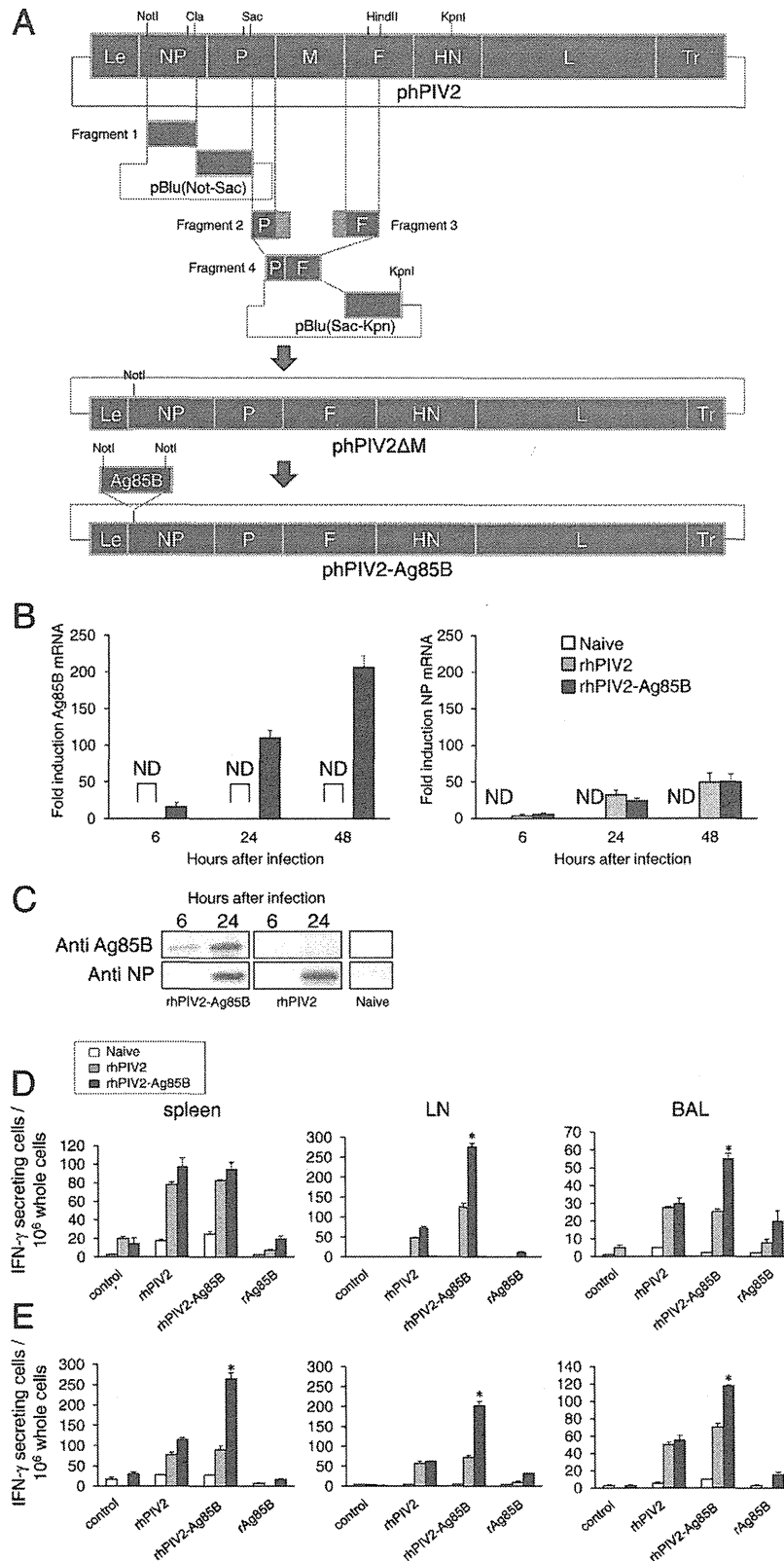
Fig. 1. Expression of Ag85B and advantageous effects in cellular immune response against Ag85B *versus* virus vector in immunized mice. (A) Construction of rhPIV2–Ag85B. (B) Expression of Ag85B (left panel) and NP (right panel) gene in BEAS cells infected with rhPIV2 or rhPIV2–Ag85B at each time point was determined by real-time PCR. Total RNA was extracted at 6, 24, and 48 h after infection. Fold increase of each target gene was normalized to β-actin, and the expression levels are represented as relative values to naïve cells. Error bars represent standard deviation. ND indicates non-detected. (C) Expression of Ag85B and NP proteins was detected by anti-Ag85B and anti-NP antibodies at 6 and 24 h after infection, respectively. (D and E) Mice were immunized 1 (D) or 2 (E) times with rhPIV2 or rhPIV2–Ag85B at a 2-week interval by intranasal

Mycobacterium bovis bacille Calmette-Guérin (BCG) has substantially contributed to the control of tuberculosis (TB) for more than 80 years and affords about 80% protection against tuberculosis meningitis and miliary tuberculosis in infant and young children. However, it is well known that the protective efficacy of BCG against pulmonary TB in adults is variable and partial [5,6]. Therefore, development of new vaccines is urgently needed for the elimination of TB as a public health threat and should be a major global public health priority.

Many infectious diseases, including TB, initially establish infection on mucosal surfaces. Therefore, the best defense against these predominantly mucosal pathogens is mucosal vaccines that are capable of inducing both systemic and mucosal immunity. However, the mucosal immune system is quite unique and is different from systemic immune responses [7,8]. Mucosal immunization provides mucosal immune responses in all mucosal effector tissues in the concept of a common mucosal immune system [9].

Human parainfluenza type 2 virus (hPIV2) is a member of the genus *Rubulavirus* of the family *Paramyxoviridae* and possesses a single-stranded, nonsegmented and negative-stranded RNA genome. This virus does not have a DNA phase during its life cycle and can avoid genetic modifications. Additionally, this virus becomes replication-incompetent by elimination of some viral genes [10]. Moreover, it is likely to lead to elicit stronger inserted antigen-specific immune responses than vector-specific responses unlike other viral vaccine vectors using inserted antigen expression mechanisms of hPIV2. In the present study, we evaluated the effectiveness of intranasal administration of Ag85B-expressed non-replicating human parainfluenza type 2 virus (rhPIV2–Ag85B), which induces weak immune responses against a viral vector, as a novel mucosal TB vaccine.

2. Materials and methods

2.1. Immunization

Six-week-old BALB/c female mice were immunized with rhPIV2–Ag85B or rhPIV2 control vector 3 or 4 times at 2-week intervals by intranasal inoculation of 1×10^8 TCID50 virus in 20 µl PBS. Another group of mice was intramuscularly immunized twice with Ag85B DNA vaccine [11] and intranasally immunized twice with rhPIV2–Ag85B. As a control group, a group of mice was vaccinated using 1×10^7 CFU of BCG Tokyo by subcutaneous injection.

2.2. Infection assay

Two weeks (rhPIV2–Ag85B-immunized mice) or 6 weeks (BCG-immunized mice) after the final immunization, mice were challenged with *M. tuberculosis* (Mtb) Kurono strain by inhalation. This bacterial preparation and infection assay were performed as previously described [12]. In brief, the mice were infected *via* the airborne route by placing them into the exposure chamber of a Glas-Col aerosol generator. The nebulizer compartment was filled with 5 ml of a suspension containing 10^6 CFU of Kurono strain so that approximately 50 bacteria would be deposited in the lungs of each animal. Eight weeks after Mtb infection, mice were sacrificed and the preventive effects of the vaccine were assessed.

2.3. Cell culture

Human bronchial epithelial cells (BEAS cells) and primary cultured normal human bronchial epithelial (NHBE) cells were obtained from the American Type Culture Collection (Manassas, VA) and Lonza (Walkersville, MD). These cells were grown in bronchial epithelial growth medium containing supplements (Lonza). These cells were infected with rhPIV2 or rhPIV2–Ag85B (MOI of 10) or treated with recombinant Ag85B (10 µg/ml) for 6–48 h in a 37 °C incubator with a 5% CO₂ atmosphere.

2.4. FACS analysis

Spleen, pulmonary lymph node (pLN), and bronchoalveolar lavage (BAL) cells were obtained from immunized mice, and single-cell suspensions were prepared. The cells were incubated with recombinant Ag85B protein (10 µg/ml final concentration) for 4 h in the presence of Brefeldin A at 37 °C with 5% CO₂. The cells were stained for surface markers with anti-CD3 and anti-CD4 (BD Biosciences, San Joes, CA) for 30 min at 4 °C, followed by fixation for 30 min at 4 °C in 2% paraformaldehyde. IFN-γ was detected by staining with anti-IFN-γ (BD Biosciences) for 30 min at 4 °C. Flow cytometry data collection was performed on a FACS Canto II (BD Biosciences). Files were analyzed using FACSDiva Software (BD Biosciences). BEAS cells infected with rhPIV2–Ag85B were stained with anti-ICAM-1 (BioLegend, San Diego, CA) and analyzed as described above.

2.5. Evaluation of Ag85B-specific immune responses by ELISPOT assay

The number of Ag85B-specific, IFN-γ-secreting cells was determined by the ELISPOT assay according to the method reported previously [11]. Triplicate samples of whole, CD4+, and CD8+ T cells (separated by a MACS system) (Miltenyi Biotec, Bergisch Gladbach, Germany) collected from the spleen, pLN, and BAL were plated at 1×10^6 cells/well. These cells were stimulated by addition of 2×10^5 mitomycin C (Sigma–Aldrich, Saint Louis, MO)-treated syngeneic spleen cells infected with recombinant vaccinia virus expressing Ag85B or rhPIV2–Ag85B.

2.6. Statistical analysis

Data are presented as means ± SD. Statistical analyses were performed using the Mann–Whitney U test. Statistically significant differences compared with the control are indicated by asterisks.

3. Results

3.1. Characteristics of rhPIV2–Ag85B

A construction of rhPIV2–Ag85B is shown in Fig. 1A. To examine gene expression levels of the inserted Ag85B, BEAS cells were infected with rhPIV2–Ag85B. Abundant and rapid expression of mRNA of Ag85B was observed in BEAS cells infected with rhPIV2–Ag85B compared with the expression of NP mRNA (Fig. 1B). These results were also confirmed by analysis of protein expression (Fig. 1C). The production of Ag85B was earlier than that of NP, which is usually the earliest synthesized protein in hPIV2 infection.

inoculation ($n = 5$ per group). Spleen, pLN, and BAL cells were collected from immunized mice ($n = 5$ per group) 2 weeks after the final immunization for examination by an ELISPOT assay. These isolated cells were stimulated *in vitro* with syngeneic spleen cells infected with control rhPIV2, rhPIV2–Ag85B, or recombinant Ag85B protein (rAg85B) (10 µg/ml final concentration) for 24 h. Error bars represent standard deviations. Statistically significant differences are indicated by asterisks (*, $P < 0.05$ compared to the group stimulated with rhPIV2).

These responses were considered to be advantageous effects in cellular immune response to inserted Ag85B *versus* rhPIV2 vector. To confirm this advantageous response, cells from immunized mice were re-stimulated *in vitro* with syngeneic spleen cells infected with rhPIV2 or rhPIV2–Ag85B. Although responses to both Ag85B and rhPIV2 vector were observed, Ag85B-specific responses were clearly seen, especially in pLN and BAL cells after single immunization (Fig. 1D). After performing immunization twice, Ag85B-specific responses were also seen in spleen cells as booster effects more than responses to the vector virus (Fig. 1E). These results indicated that rhPIV2–Ag85B immunization elicited inserted Ag85B-specific immune responses without being hidden by vector responses.

3.2. Intranasal administration of rhPIV2–Ag85B prevents infection with Mtb in mice

To investigate the ability of intranasal administration of rhPIV2–Ag85B to elicit a protective effect against pulmonary TB, rhPIV2–Ag85B-immunized mice were aerosol-infected with highly pathogenic Mtb kurono strain [13]. One group of mice were intranasally immunized with rhPIV2–Ag85B 4 times at 2-week intervals, and another group of mice were intranasally immunized with rhPIV2–Ag85B twice following intramuscular immunization with Ag85B DNA twice (Fig. 2A). Intranasal administration of rhPIV2–Ag85B resulted in a decreases in granulomatous lesions and inflammatory area. However, there were no apparent histopathological differences, such as infiltrating cell types, between the each group of mice, and these results are similar to the results of another study focusing on TB vaccine [14]. On the other hand, these vaccine effects were clearly seen by staining for acid-fast bacillus. Mice immunized with rhPIV2–Ag85B showed a substantial reduction in the infiltration of bacteria, and this inhibitory effect on bacterial expansion was correlated with the number of rhPIV2–Ag85B intranasal administrations (Fig. 2B). CFU of Mtb in spleens from both groups of immunized mice was also significantly lower than those in mice immunized with the control vector (Fig. 2C). As for a preventive effect on Mtb infection in the lung, the mice immunized with rhPIV2–Ag85B clearly showed a substantial reduction in CFU.

3.3. Ag85B-specific immune response is elicited by rhPIV2–Ag85B administration

The capacity of rhPIV2–Ag85B intranasal immunization to elicit effector cells that recognize endogenously expressed Ag85B was assessed. Spleen, pLN, and BAL cells obtained from immunized mice were re-stimulated *in vitro* with syngeneic spleen cells infected with the recombinant vaccinia virus expressing Ag85B, and endogenously expressed Ag85B-specific cellular immune response was examined by ELISPOT assays. Both CD4+ and CD8+ splenocytes exhibited Ag85B-specific responses, and CD8+ T cells showed much stronger responses than those of CD4+ T cells in splenocytes from mice immunized with rhPIV2–Ag85B (Fig. 3A). Ag85B-specific responses were also seen in both CD4+ and CD8+ T cells at almost the same levels in pLN and BAL cells (Fig. 3B and C).

3.4. Analysis of Ag-specific effector cells and immune responses in pLN cells and the lung

Delayed initial activation of effector cells in lungs has been reported in the case of Mtb infection [15]. To control bacterial expansion in the early phase of infection, rapid Mtb Ag-specific CD4+ T cell responses are required. Thus, we next analyzed recruitment of Ag85B-specific IFN-γ+ CD4+ T cells in pLN and BAL cells in mice immunized with rhPIV2–Ag85B. Mice were intranasally immunized with rhPIV2–Ag85B or the control vector virus 3 times
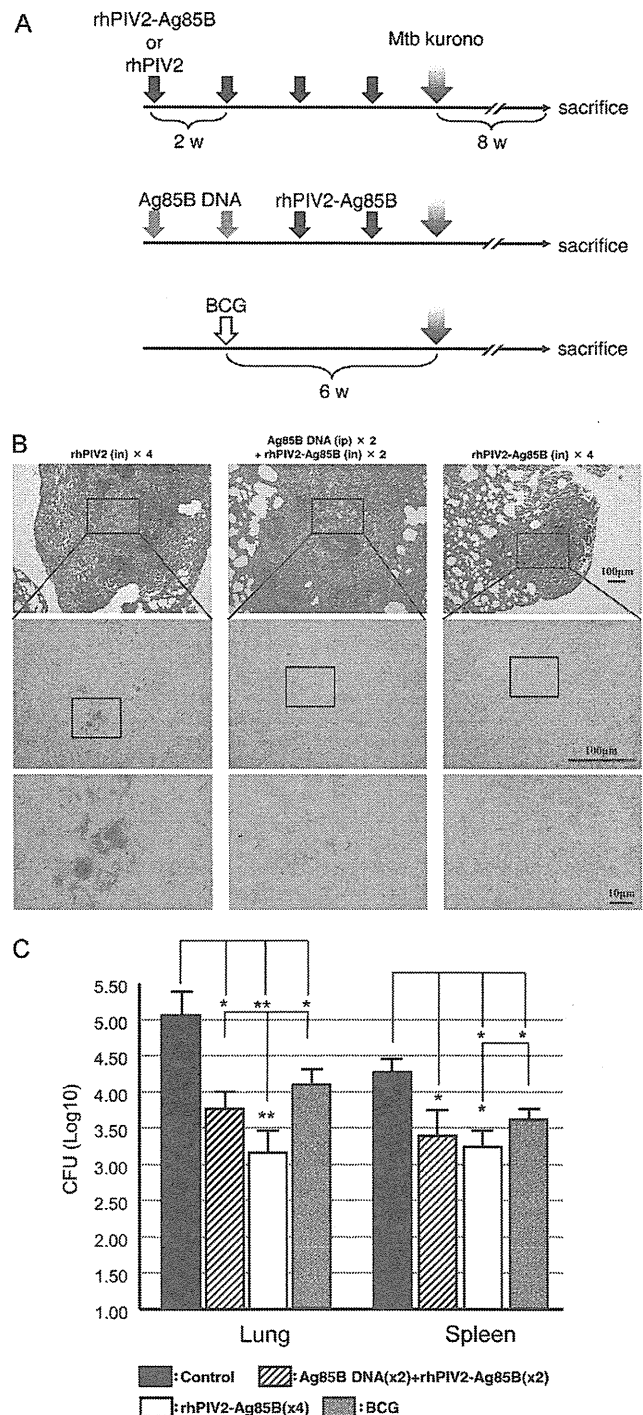
Fig. 2. Repeated immunization with rhPIV2–Ag85B results in protection from TB. (A) Groups of mice were vaccinated in this schedule. (B) Histological images of the lungs of Mtb-infected mice. Groups of mice (n = 10) immunized 4 times with rhPIV2 (left panel), 2 times with Ag85B DNA vaccine and 2 times with rhPIV2–Ag85B (middle panel) or 4 times with rhPIV2–Ag85B (right panel) were challenged by Mtb infection. Arrows point to tubercles. Lower panels in (B) show magnified images of images in the middle panels. (C) Inhibition of bacterial growth by immunization with rhPIV2–Ag85B in the lung and spleen. Groups of mice immunized 2 times with Ag85B DNA vaccine and 2 times with rhPIV2–Ag85B or immunized 4 times with rhPIV2–Ag85B or BCG were challenged by Mtb infection. The numbers of Mtb CFU in the lung and spleen were determined by a colony enumeration assay. The bacterial load is represented as mean $\log_{10}$ CFU per organ. Error bars represent standard deviations. Statistically significant differences are indicated by asterisks (*, $P < 0.05$, **, $P < 0.005$).
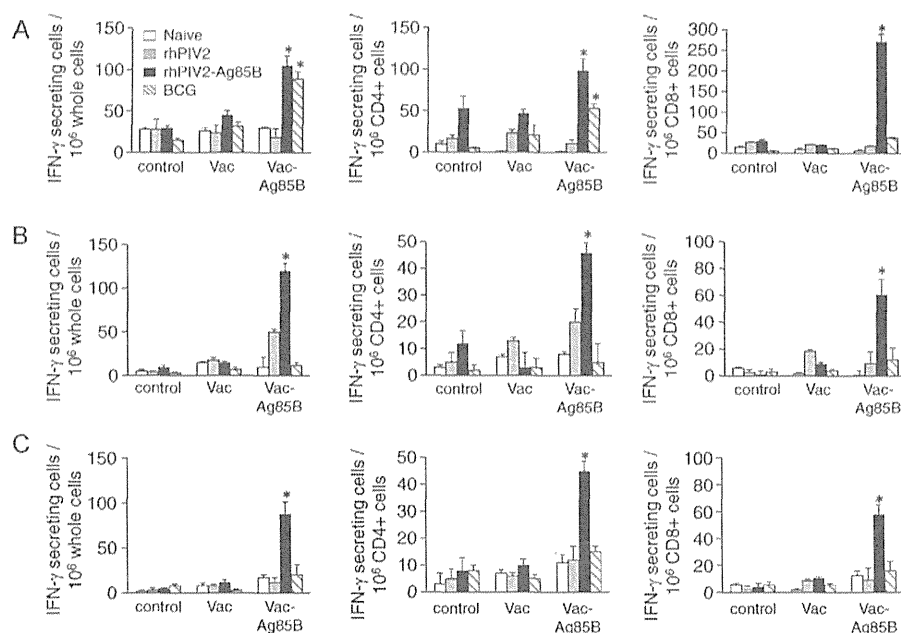
Fig. 3. Induction of Ag85B-specific cellular immune responses in rhPIV2-Ag85B-immunized mice. Mice were immunized with rhPIV2, rhPIV2-Ag85B, or BCG (n = 5 per group) according to the schedule shown in Fig. 2A. Two (rhPIV2 or rhPIV2-Ag85B) or 4 weeks (BCG) after the final immunization, the spleen, pLN, and BAL were collected. Isolated cells from the spleen (A), pLN (B), or BAL (C) were separated into whole (left panels), CD4$^+$ (middle panels), and CD8$^+$ (right panels) T cells and examined for IFN-γ production in an ELISPOT assay. These cells were stimulated in vitro with syngeneic spleen cells infected with control vaccinia virus (Vac) or recombinant vaccinia virus carrying the Ag85B gene (Vac-Ag85B) for 24 h. Error bars represent standard deviations. Statistically significant differences are indicated by asterisks (*, P < 0.01 compared to the group stimulated with Vac).

at 2-week intervals. Another group of mice were immunized with BCG by subcutaneous injection. Two weeks (rhPIV2-Ag85B-immunized mice) or 6 weeks (BCG-immunized mice) after the final immunization, all mice were challenged with Mtb Kurono strain by inhalation (Fig. 4A). At each time point after immunization or Mtb challenge, the percentage and absolute number of Ag85B-specific IFN-γ^+ CD4$^+$ cells were determined by flow cytometry. Before Mtb challenge, the percentage of IFN-γ^+ CD4$^+$ cells in pLN cells was increased by immunization with rhPIV2-Ag85B but not by BCG immunization (Fig. 4B and C, top). However, a significant increase in IFN-γ^+ CD4$^+$ cells was not detected in BAL cells (Fig. 4B and C, bottom). Interestingly, expansion of IFN-γ^+ CD4$^+$ cells occurred after Mtb challenge in BAL cells more dramatically than that in pLN cells in terms of absolute number (Fig. 4C). These responses induced by rhPIV2-Ag85B immunization were much stronger than those induced by BCG immunization.

Similarly, an increase in Ag85B-specific responses was observed by the ELISPOT assay (Fig. 4D). The number of Ag85B-specific IFN-γ secreting cells increased in pLN cells from mice immunized with rhPIV2-Ag85B in a number of immunizations-dependent manner. Furthermore, strong Ag85B-specific responses were detected after Mtb challenge in pLN and BAL cells, and the responses were much stronger than those in BCG immunized mice.

3.5. rhPIV2–Ag85B induces innate immune responses

We explored innate immune responses induced by rhPIV2-Ag85B infection. We confirmed that Ag85B did not affect the viability of rhPIV2-Ag85B infected cells (Supplemental Fig. 1) [44–46]. Type I IFNs were assessed after infection with rhPIV2-Ag85B in NHBE and BEAS cells as an indication of innate immune responses. Both types of cells showed mRNA expression of type I IFNs after infection with rhPIV2-Ag85B but not after addition of recombinant Ag85B protein (Fig. 5A). Production of IFN-β was also detected in the culture supernatant by ELISA

(Fig. 5B). The mRNA expression of intracellular receptors, RIG-I, MDA5, and TLR3, and the induction of cytokines, IL-6 and IL-15 were also enhanced by infection with rhPIV2-Ag85B, whereas these effects were not observed with the addition of recombinant Ag85B protein (Fig. 5C and D). Furthermore, the expression of ICAM-1 was induced by infection with rhPIV2-Ag85B (Fig. 5E). Similar results were obtained after infection with rhPIV2 vector alone or rhPIV2-GFP (Supplemental Fig. 2). Other co-stimulation molecules, CD80, CD86, ICAM-2 and selectin, were not detected (data not shown).

To further investigate the participation of these receptors in innate immune activation induced by rhPIV2-Ag85B infection, expression of these receptors was knocked down by transfecting siRNA. At 48 h after transfection with siRNA, expression levels of these receptors were reduced by approximately 90% or expression was no longer detectable (Fig. 5F). IFN-β production induced by rhPIV2-Ag85B infection was inhibited when the cells were treated with RIG-I siRNA. For other receptors, MDA5 and TLR3, siRNA treatment did not result in inhibition of IFN-β production induced by rhPIV2-Ag85B infection (Fig. 5G). This result was confirmed by phosphorylation of IRF3, which is a downstream molecule of RIG-I in epithelial cells. The phosphorylation of IRF3 induced by rhPIV2-Ag85B infection was inhibited when epithelial cells were treated with siRNA of RIG-I (Fig. 5H).

4. Discussion

In the present study, we demonstrated the effectiveness of hPIV2 vectors for TB vaccines to induce systemic and mucosal immune responses. The rhPIV2 vector is a weak immunogenic; however, intranasal immunization with rhPIV2-Ag85B showed more potent protection against pulmonary TB in BALB/c mice than did conventional BCG vaccination. The rhPIV2-Ag85B shows a vaccine effect by itself alone, and this effect is more useful than the effects of other vectors for TB vaccines.
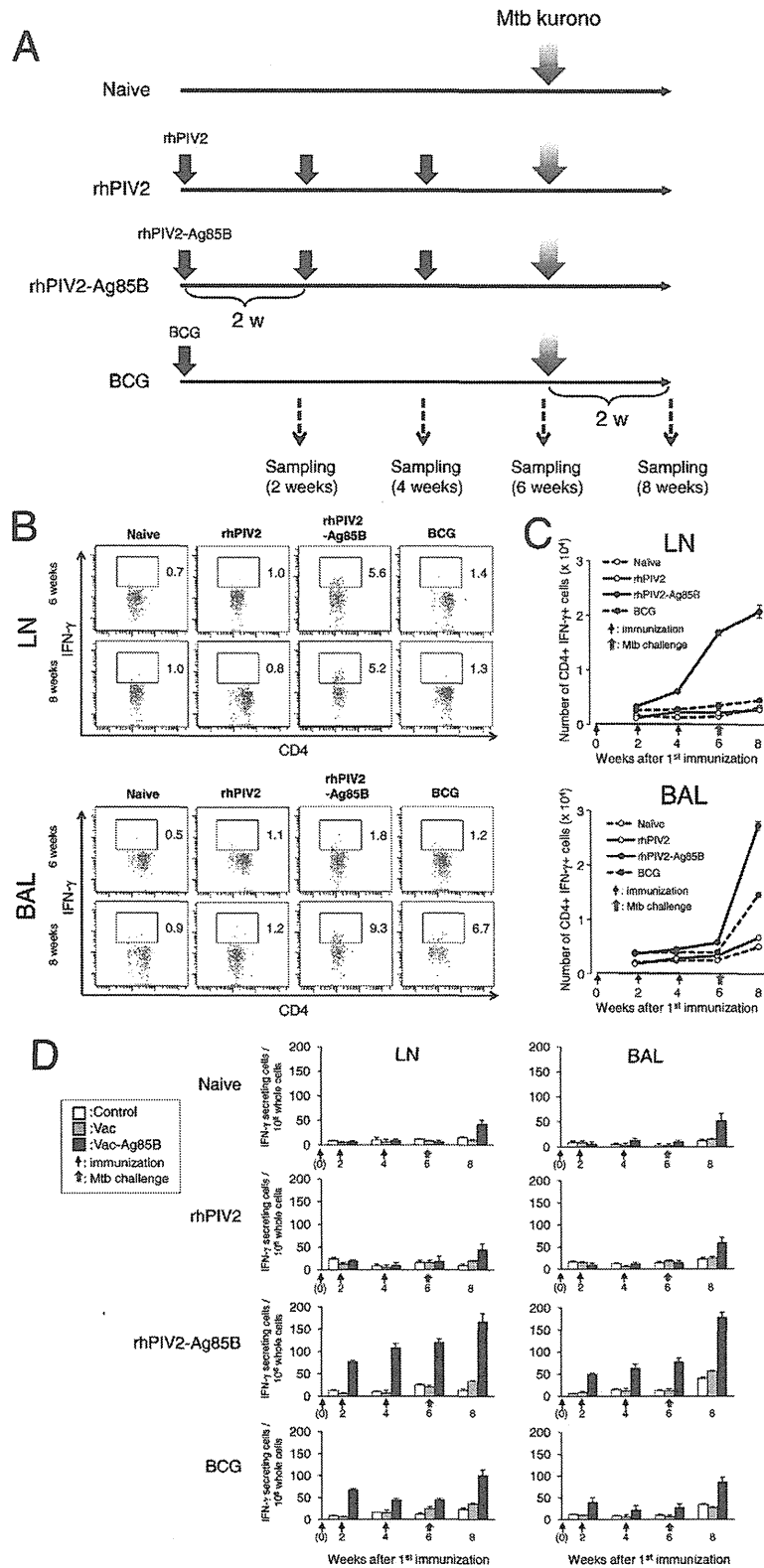
Fig. 4. Analysis of Ag-specific effector cells and these immune responses in pLN and BAL. (A) Groups of mice were immunized with rhPIV2, rhPIV2–Ag85B, or BCG (n = 10 per group) and challenged by Mtb infection in this schedule. (B) Representative flow cytometry plots of IFN-γ^+ cells on gated CD4$^+$ cells from pLN (top panels) and BAL (bottom panels) are shown. Numbers shown beside the gates represent the percentages within CD4$^+$ T cells. (C) Kinetics of recruitment of Ag85B-specific IFN-γ^+ cells in pLN (top panel) and BAL (bottom panel). Absolute numbers of IFN-γ^+ CD4$^+$ cell populations at each time points are shown. Error bars represent standard deviations. (D) Isolated cells from the pLN and BAL at each time point were examined for IFN-γ production in an ELISPOT assay. These cells were stimulated *in vitro* with syngeneic spleen cells infected with control vaccinia virus (Vac) or recombinant vaccinia virus carrying the Ag85B gene (Vac-Ag85B) for 24 h. Error bars represent standard deviations.
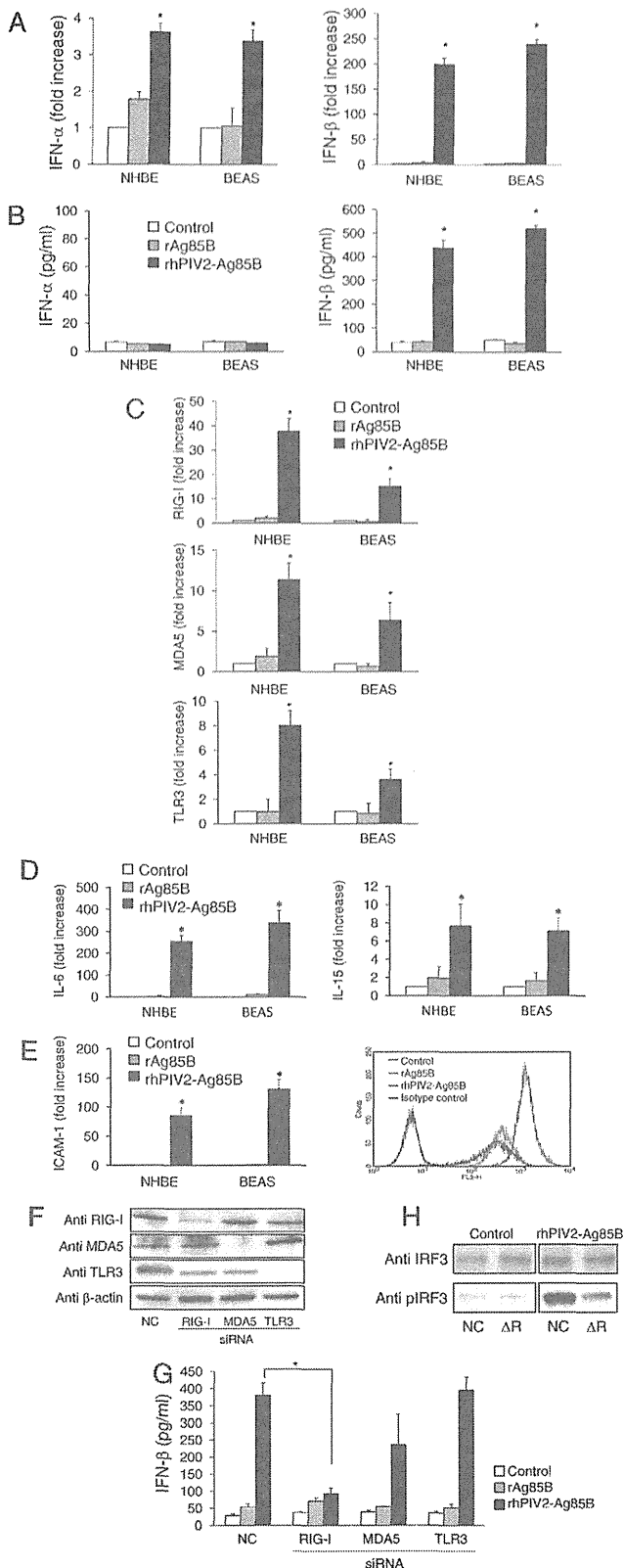
Fig. 5. Evaluation of adjuvant activity of rhPIV2–Ag85B in vitro. NHBE and BEAS cells were treated with rAg85B protein (10 μg/ml) or infected with rhPIV2–Ag85B (MOI of 10) for 24 h, and the increases in mRNA levels of IFN-α, IFN-β (A), RIG-I, MDA5, TLR3 (C), IL-6, IL-15 (D), and ICAM-1 (E, left panel) were determined by real-time PCR. Fold increase of each target gene was normalized to β-actin, and the

Viral vectors are promising vaccine candidates for eliciting Ag-specific immune responses [16,17]. Pre-existing anti-vector antibodies, however, constitute an obstacle for use in humans [18–20]. Although antibodies against hPIV are known to cross-react with Sendai virus, Sendai virus vector is considered to be effective for human use by intranasal administration [21]. Additionally, Sendai virus vector is not affected by antibodies against Sendai virus for induction of T cell responses, especially when it is administered intranasally [4]. From these findings, intranasal administration of the hPIV2 vector is also considered to be effective for human use. In fact, multiple administrations with rhPIV2–Ag85B also showed preventive effects more clearly than did immunization 2 times with rhPIV2–Ag85B (Fig. 2).

Many viral vectors have been tested as recombinant viral vaccines eliciting suitable recombinant Ag-specific immune responses, and many of these vaccine vectors are not vaccine viruses such as vaccinia virus Ankara (MVA), adenovirus, Sendai virus, and CMV. These viral vectors have also been used in several vaccine trials in TB or HIV vaccine [22–24]. Experience in the HIV vaccine field has emphasized the importance of avoiding anti-vector immune responses when developing a vectored vaccine [25]. Immune responses to vaccine vectors prevent the induction of aimed immune responses against recombinant Ag. From these findings, elimination of the immunogenicity of a vaccine vector is critical for a recombinant viral vaccine. The immunogenicity of viral vectors depends on the amount of vector viral proteins. Approximately 80 poxvirus proteins are encoded by its over 130–300 kbp and the adenovirus genome sizes are 26–45 kbp. The genome sizes of these two viral vectors are much larger than that of hPIV2 (15.65 kbp), and induction of immune responses to hPIV2 vector might be lower than other viral vectors. In TB vaccines, recombinant vaccinia virus and adenovirus, which are immunogenic viruses, did not show clear vaccine effects against TB infection by immunization with themselves alone. These two recombinant TB vaccines, adenovirus and MVA, were utilized as boost immunization after BCG priming [26,27]. These heterologous prime-boost strategies diminish immune responses to the vector virus and indicate the possibility of a practical and efficient strategy for prevention of TB [28,29]. On the other hand, the most common method for obtaining an attenuated virus is gene elimination of the viral construct protein to make a replication-deficient virus in vivo. The rhPIV2 vector is a weak immunogenicity by elimination of structural protein (M) gene; however, the rhPIV2–Ag85B shows a vaccine effect by immunization with itself alone, and this effect is more useful than the effects of other vectors for a recombinant TB vaccine.

The hPIV2 vector has an additional advantage over other viral vectors. The inserted Ag85B gene, which is only 978 bp, is a minor component of rhPIV2–Ag85B. Despite that, the cellular immune response against Ag85B had an advantage over that against the virus vector in mice. This advantageous effect is thought to depend

expression levels are represented as relative values to the control. Culture supernatants were also collected, and amounts of secreted IFN-α and IFN-β were measured by ELISA (B). Expression of ICAM-1 was also confirmed by FACS analysis in BEAS cells (E, right panel). Data are averages of triplicate samples from three identical experiments, and error bars represent standard deviations. Statistically significant differences between control cells and rhPIV2–Ag85B-infected cells are indicated by asterisks (*, P < 0.01). BEAS cells were treated with siRNA targeting RIG-I, MDA5, TLR3, or the negative control siRNA (NC) for 48 h. Depletion of them was examined by immunoblotting (F). Those cells were stimulated by rAg85B protein (10 μg/ml) or infected with rhPIV2–Ag85B (MOI of 10) and then production of IFN-β was measured by ELISA (G). Data are averages of triplicate samples from three identical experiments, and error bars represent standard deviations. Statistically significant differences are indicated by asterisks (*, P < 0.01 compared to NC). The effects of depletion of RIG-I on IRF3 phosphorylation were tested. BEAS cells treated with NC or siRNA targeting RIG-I (ΔR) for 48 h were infected with rhPIV2–Ag85B or not infected (control). Whole IRF3 and phosphorylated IRF3 (pIRF3) were detected by immunoblotting 6 h after infection (H).

on Ag85B expression mechanisms. The frequency with which viral RNA polymerase reinitiates the next mRNA at gene junctions is imperfect, and this leads to a gradient of mRNA abundance that decreases according to distance from the genome 3' end [30]. Insertion of the Ag85B gene into the 3' proximal first locus between the leader sequence and the NP gene results in the highest level of gene expression. Ag85B is transcribed earlier and more abundantly than other viral products (Fig. 1B and C). This property of rhPIV2–Ag85B leads to elicit stronger Ag85B-specific immune responses than vector-specific responses in our system (Fig. 1D and E), although recombinant virus vaccine immunization usually induces overwhelming viral-specific immune responses compared with an inserted gene product [31,32]. We also demonstrated that intranasal administration of the rhPIV2 vector had no adverse effects and provided sufficient immunogenicity and a sufficient vaccine effect against Mtb in mice. These results suggest that intranasal administration of rhPIV2–Ag85B does not cause functional failure as a vaccine by multiple administrations, and these features of the rhPIV2 vector are definitely advantages for clinical use.

Another major feature of rhPIV2–Ag85B is effective prevention of TB by intranasal administration. Vaccination in the respiratory tract may enhance protection against Mtb infection, since Mtb initially establishes infection on mucosal surfaces of the respiratory tract. Indeed, a number of recombinant TB vaccines have been developed and evaluated for respiratory mucosal immunization [33–35]. It is important to note that lack of Ag-specific effector cells persists even up to about 21 days after pulmonary Mtb infection caused by a bacterial component [15,36]. In the present study, the arrival of Ag-specific T cells was detected in lung and pLN by rhPIV2–Ag85B immunization, and this arrival of effector cells was recognized faster than BCG immunization after Mtb challenge (Fig. 4B and C). We were able to establish a novel intranasal vaccine, rhPIV2–Ag85B, against TB by utilizing various advantages of intranasal administration. Nasal administration of a vaccine to induce mucosal and systemic immune responses has several advantages other than the induction of effective immune responses. It is even possible that intranasal administration of replication-incompetent rhPIV2–Ag85B limits the areas of infection in respiratory organs and induces a respiratory tract mucosal immune response in addition to a systemic immune response against TB. Our study suggested that intranasal administration of rhPIV2–Ag85B, which can induce both mucosal and systemic immune responses against Mtb, has a great advantage as a TB vaccine.

Attempts have been made to use various types of adjuvants for enhancing an immune responses to vaccines, including vaccines against TB [37]. In fact, a protein-based TB vaccine required the addition of an adjuvant to induce effective immune responses [38–41]. For the generation of adaptive immune responses, induction of innate immunity is crucial for vaccines to elicit potent Ag-specific immune responses. Pattern recognition receptors have been studied as potential targets for an adjuvant. dsRNA is a dominant activator of innate immunity because viral dsRNA is recognized by TLR3, RIG-I, and MDA5 [42,43]. As a result, it was demonstrated that the rhPIV2 vector had a potent adjuvant activity as dsRNA recognized by the RIG-I receptor and enhanced not only local innate immunity but also systemic adaptive immunity. It is possible that no extra addition of an adjuvant is required to prevent TB by vaccination with rhPIV2–Ag85B. Furthermore, the inhibitory effects on the growth of rhPIV2–Ag85B *in vivo* by IFN through the innate receptor are not required to consider since the rhPIV2 vector is replication-incompetent *in vivo* by elimination of the M gene (Fig. 1A).

In summary, our results provide evidence for the possibility of rhPIV2–Ag85B as a novel intranasal vaccine for eliciting

Mtb-specific mucosal immunity. Immunization with rhPIV2–Ag85B showed significant protection against TB without any prime vaccine or addition of an adjuvant in mice. Further studies will contribute to the ultimate goal of establishing a new vaccine strategy that can definitely prevent Mtb infection.

Appendix A. Supplementary data

Supplementary material related to this article can be found, in the online version, at http://dx.doi.org/10.1016/j.vaccine.2013.11.108.

References

[1] Small JC, Ertl HC. Viruses – from pathogens to vaccine carriers. Curr Opin Virol 2011;1(October (4)):241–5.

[2] Halle S, Dujardin HC, Bakocevic N, Fleige H, Danzer H, Willenzon S, et al. Induced bronchus-associated lymphoid tissue serves as a general priming site for T cells and is maintained by dendritic cells. J Exp Med 2009;206(November (12)):2593–601.

[3] Okano S, Yonemitsu Y, Shirabe K, Kakeji Y, Maehara Y, Harada M, et al. Provision of continuous maturation signaling to dendritic cells by RIG-I-stimulating cytosolic RNA synthesis of Sendai virus. J Immunol 2011;186(February (3)):1828–39.

[4] Moriya C, Horiba S, Kurihara K, Kamada T, Takahara Y, Inoue M, et al. Intranasal Sendai viral vector vaccination is more immunogenic than intramuscular under pre-existing anti-vector antibodies. Vaccine 2011;29(November (47)):8557–63.

[5] Randomised controlled trial of single BCG, repeated BCG, or combined BCG and killed Mycobacterium leprae vaccine for prevention of leprosy and tuberculosis in Malawi. Karonga Prevention Trial Group. Lancet 1996;348(July (9019)):17–24.

[6] Rodrigues LC, Pereira SM, Cunha SS, Genser B, Ichihara MY, de Brito SC, et al. Effect of BCG revaccination on incidence of tuberculosis in school-aged children in Brazil: the BCG-REVAC cluster-randomised trial. Lancet 2005;366(October (9493)):1290–5.

[7] Zinselmeyer BH, Dempster J, Gurney AM, Wokosin D, Miller M, Ho H, et al. In situ characterization of CD4+ T cell behavior in mucosal and systemic lymphoid tissues during the induction of oral priming and tolerance. J Exp Med 2005;201(June (11)):1815–23.

[8] Dwivedy A, Aich P. Importance of innate mucosal immunity and the promises it holds. Int J Gen Med 2011;4:299–311.

[9] Kiyono H, Kweon MN, Hiroi T, Takahashi I. The mucosal immune system: from specialized immune defense to inflammation and allergy. Acta Odontol Scand 2001;59(June (3)):145–53.

[10] Kawano M, Kaito M, Kozuka Y, Komada H, Noda N, Nanba K, et al. Recovery of infectious human parainfluenza type 2 virus from cDNA clones and properties of the defective virus without V-specific cysteine-rich domain. Virology 2001;284(May (1)):99–112.

[11] Takamura S, Matsuo K, Takebe Y, Yasutomi Y. Ag85B of mycobacteria elicits effective CTL responses through activation of robust Th1 immunity as a novel adjuvant in DNA vaccine. J Immunol 2005;175(August (4)):2541–7.

[12] Sugawara I, Mizuno S, Yamada H, Matsumoto M, Akira S. Disruption of nuclear factor-interleukin-6, a transcription factor, results in severe mycobacterial infection. Am J Pathol 2001;158(February (2)):361–6.

[13] Sugawara I, Yamada H, Kazumi Y, Doi N, Otomo K, Aoki T, et al. Induction of granulomas in interferon-gamma gene-disrupted mice by avirulent but not by virulent strains of Mycobacterium tuberculosis. J Med Microbiol 1998;47(October (10)):871–7.

[14] Sweeney KA, Dao DN, Goldberg MF, Hsu T, Venkataswamy MM, Henao-Tamayo M, et al. A recombinant Mycobacterium smegmatis induces potent bactericidal immunity against Mycobacterium tuberculosis. Nat Med 2011;17(October (10)):1261–8.

[15] Shafiani S, Tucker-Heard G, Kariyone A, Takatsu K, Urdahl KB. Pathogen-specific regulatory T cells delay the arrival of effector T cells in the lung during early tuberculosis. J Exp Med 2010;207(July (7)):1409–20.

[16] Draper SJ, Heeney JL. Viruses as vaccine vectors for infectious diseases and cancer. Nat Rev Microbiol 2010;8(January (1)):62–73.

[17] Clark KR, Johnson PR. Gene delivery of vaccines for infectious disease. Curr Opin Mol Ther 2001;3(August (4)):375–84.

[18] Sumida SM, Truitt DM, Lemckert AA, Vogels R, Custers JH, Addo MM, et al. Neutralizing antibodies to adenovirus serotype 5 vaccine vectors are directed primarily against the adenovirus hexon protein. J Immunol 2005;174(June (11)):7179–85.

[19] Catanzaro AT, Koup RA, Roederer M, Bailer RT, Enama ME, Moodie Z, et al. Phase 1 safety and immunogenicity evaluation of a multiclade HIV-1 candidate vaccine delivered by a replication-defective recombinant adenovirus vector. J Infect Dis 2006;194(December (12)):1638–49.

[20] Priddy FH, Brown D, Kublin J, Monahan K, Wright DP, Lalezari J, et al. Safety and immunogenicity of a replication-incompetent adenovirus type 5 HIV-1 clade B gag/pol/nef vaccine in healthy adults. Clin Infect Dis 2008;46(June (11)):1769–81.

[21] Hara H, Hironaka T, Inoue M, Iida A, Shu T, Hasegawa M, et al. Prevalence of specific neutralizing antibodies against Sendai virus in populations from different geographic areas: implications for AIDS vaccine development using Sendai virus vectors. Hum Vaccin 2011;7(June (6)):639–45.

[22] McShane H, Brookes R, Gilbert SC, Hill AV. Enhanced immunogenicity of CD4(+) t-cell responses and protective efficacy of a DNA-modified vaccinia virus Ankara prime-boost vaccination regimen for murine tuberculosis. Infect Immun 2001;69(February (2)):681–6.

[23] Radosevic K, Wieland CW, Rodriguez A, Weverling GJ, Mintardjo R, Gillissen G, et al. Protective immune responses to a recombinant adenovirus type 35 tuberculosis vaccine in two mouse strains: CD4 and CD8 T-cell epitope mapping and role of gamma interferon. Infect Immun 2007;75(August (8)):4105–15.

[24] Munier CM, Andersen CR, Kelleher AD. HIV vaccines: progress to date. Drugs 2011;71(March (4)):387–414.

[25] Cheng C, Wang L, Gall JG, Nason M, Schwartz RM, McElrath MJ, et al. Decreased pre-existing Ad5 capsid and Ad35 neutralizing antibodies increase HIV-1 infection risk in the Step trial independent of vaccination. PLoS ONE 2012;7(4):e33969.

[26] Abel B, Tameris M, Mansoor N, Gelderbloem S, Hughes J, Abrahams D, et al. The novel tuberculosis vaccine, AERAS-402, induces robust and polyfunctional CD4+ and CD8+ T cells in adults. Am J Respir Crit Care Med 2010;181(June (12)):1407–17.

[27] McShane H, Pathan AA, Sander CR, Keating SM, Gilbert SC, Huygen K, et al. Recombinant modified vaccinia virus Ankara expressing antigen 85A boosts BCG-primed and naturally acquired antimycobacterial immunity in humans. Nat Med 2004;10(November (11)):1240–4.

[28] Rahman S, Magalhaes I, Rahman J, Ahmed RK, Sizemore DR, Scanga CA, et al. Prime-boost vaccination with rBCG/rAd35 enhances CD8(+) cytolytic T-cell responses in lesions from Mycobacterium tuberculosis-infected primates. Mol Med 2012;18:647–58.

[29] Pathan AA, Minassian AM, Sander CR, Rowland R, Porter DW, Poulton ID, et al. Effect of vaccine dose on the safety and immunogenicity of a candidate TB vaccine, MVA85A, in BCG vaccinated UK adults. Vaccine 2012;30(August (38)):5616–24.

[30] Tokusumi T, Iida A, Hirata T, Kato A, Nagai Y, Hasegawa M. Recombinant Sendai viruses expressing different levels of a foreign reporter gene. Virus Res 2002;86(June (1–2)):33–8.

[31] Sakurai H, Kawabata K, Sakurai F, Nakagawa S, Mizuguchi H. Innate immune response induced by gene delivery vectors. Int J Pharm 2008;354(April (1–2)):9–15.

[32] Chen D, Murphy B, Sung R, Bromberg JS. Adaptive and innate immune responses to gene transfer vectors: role of cytokines and chemokines in vector function. Gene Ther 2003;10(June (11)):991–8.

[33] Wang J, Thorson L, Stokes RW, Santosuosso M, Huygen K, Zganiacz A, et al. Single mucosal, but not parenteral, immunization with recombinant adenoviral-based vaccine provides potent protection from pulmonary tuberculosis. J Immunol 2004;173(November (10)):6357–65.

[34] Dietrich J, Andersen C, Rappuoli R, Doherty TM, Jensen CG, Andersen P. Mucosal administration of Ag85B-ESAT-6 protects against infection with Mycobacterium tuberculosis and boosts prior bacillus Calmette-Guerin immunity. J Immunol 2006;177(November (9)):6353–60.

[35] Ballester M, Nembrini C, Dhar N, de Titta A, de Piano C, Pasquier M, et al. Nanoparticle conjugation and pulmonary delivery enhance the protective efficacy of Ag85B and CpG against tuberculosis. Vaccine 2011;29(September (40)):6959–66.

[36] Wolf AJ, Desvignes L, Linas B, Banaiee N, Tamura T, Takatsu K, et al. Initiation of the adaptive immune response to Mycobacterium tuberculosis depends on antigen production in the local lymph node, not the lungs. J Exp Med 2008;205(January (1)):105–15.

[37] Moreno-Mendieta SA, Rocha-Zavaleta L, Rodriguez-Sanoja R. Adjuvants in tuberculosis vaccine development. FEMS Immunol Med Microbiol 2010;58(February (1)):75–84.

[38] Lin PL, Dietrich J, Tan E, Abalos RM, Burgos J, Bigbee C, et al. The multistage vaccine H56 boosts the effects of BCG to protect cynomolgus macaques against active tuberculosis and reactivation of latent Mycobacterium tuberculosis infection. J Clin Invest 2012;122(January (1)):303–14.

[39] Aagaard C, Hoang T, Dietrich J, Cardona PJ, Izzo A, Dolganov G, et al. A multistage tuberculosis vaccine that confers efficient protection before and after exposure. Nat Med 2011;17(February (2)):189–94.

[40] Bertholet S, Ireton GC, Ordway DJ, Windish HP, Pine SO, Kahn M, et al. A defined tuberculosis vaccine candidate boosts BCG and protects against multidrug-resistant Mycobacterium tuberculosis. Sci Transl Med 2010;2(October (53)):53ra74.

[41] Von Eschen K, Morrison R, Braun M, Ofori-Anyinam O, De Kock E, Pavithran P, et al. The candidate tuberculosis vaccine Mtb72F/AS02A: tolerability and immunogenicity in humans. Hum Vaccine 2009;5(July (7)):475–82.

[42] Alexopoulou L, Holt AC, Medzhitov R, Flavell RA. Recognition of double-stranded RNA and activation of NF-kappaB by Toll-like receptor 3. Nature 2001;413(October (6857)):732–8.

[43] Kato H, Takeuchi O, Sato S, Yoneyama M, Yamamoto M, Matsui K, et al. Differential roles of MDA5 and RIG-I helicases in the recognition of RNA viruses. Nature 2006;441(May (7089)):101–5.

[44] Buchholz UJ, Finke S, Conzelmann KK. Generation of bovine respiratory syncytial virus (BRSV) from cDNA: BRSV NS2 is not essential for virus replication in tissue culture, and the human RSV leader region acts as a functional BRSV genome promoter. J Virol 1999;73(January (1)):251–9.

[45] Yasui F, Kai C, Kitabatake M, Inoue S, Yoneda M, Yokochi S, et al. Prior immunization with severe acute respiratory syndrome (SARS)-associated coronavirus (SARS-CoV) nucleocapsid protein causes severe pneumonia in mice infected with SARS-CoV. J Immunol 2008;181(November (9)):6337–48.

[46] Falkner FG, Moss B. Escherichia coli gpt gene provides dominant selection for vaccinia virus open reading frame expression vectors. J Virol 1988;62(June (6)):1849–54.

Nonagonistic Dectin-1 ligand transforms CpG into a multitask nanoparticulate TLR9 agonist

Kouji Kobiyama[a,b], Taiki Aoshi[a,b], Hirotaka Narita[c], Etsushi Kuroda[a,b], Masayuki Hayashi[a,b], Kohhei Tetsutani[a,b], Shohei Koyama[d,e], Shinichi Mochizuki[f], Kazuo Sakurai[f], Yuko Katakai[g], Yasuhiro Yasutomi[h], Shinobu Saijo[i,j], Yoichiro Iwakura[k], Shizuo Akira[l], Cevayir Coban[m], and Ken J. Ishii[a,b,1]

[a]Laboratory of Adjuvant Innovation, National Institute of Biomedical Innovation, Osaka 567-0085, Japan; Laboratories of [b]Vaccine Science, [l]Host Defense, and [m]Malaria Immunology, World Premier International Immunology Frontier Research Center and [c]Supramolecular Crystallography, Research Center for Structural and Functional Proteomics, Institute for Protein Research, Osaka University, Osaka 565-0871, Japan; [d]Department of Medical Oncology and [e]Cancer Vaccine Center, Dana-Farber Cancer Institute, Boston, MA 02115; [f]Department of Chemistry and Biochemistry, University of Kitakyushu, Fukuoka 808-0135, Japan; [g]Corporation for Production and Research of Laboratory Primates, Ibaraki 305-0843, Japan; [h]Tsukuba Primate Research Center, National Institute of Biomedical Innovation, Ibaraki 305-0843, Japan; [i]Department of Molecular Immunology, Medical Mycology Research Center, Chiba University, Chiba 260-8673, Japan; [j]Precursory Research for Embryonic Science and Technology, Japan Science and Technology Agency, Saitama 332-0012, Japan; and [k]Division of Experimental Animal Immunology, Research Institute for Biomedical Sciences, Tokyo University of Science, Chiba 278-8510, Japan

CpG DNA, a ligand for Toll-like receptor 9 (TLR9), has been one of the most promising immunotherapeutic agents. Although there are several types of potent humanized CpG oligodeoxynucleotide (ODN), developing "all-in-one" CpG ODNs activating both B cells and plasmacytoid dendritic cells forming a stable nanoparticle without aggregation has not been successful. In this study, we generated a novel nanoparticulate K CpG ODN (K3) wrapped by the nonagonistic Dectin-1 ligand schizophyllan (SPG), K3-SPG. In sharp contrast to K3 alone, K3-SPG stimulates human peripheral blood mononuclear cells to produce a large amount of both type I and type II IFN, targeting the same endosome where IFN-inducing D CpG ODN resides without losing its K-type activity. K3-SPG thus became a potent adjuvant for induction of both humoral and cellular immune responses, particularly CTL induction, to coadministered protein antigens without conjugation. Such potent adjuvant activity of K3-SPG is attributed to its nature of being a nanoparticle rather than targeting Dectin-1 by SPG, accumulating and activating antigen-bearing macrophages and dendritic cells in the draining lymph node. K3-SPG acting as an influenza vaccine adjuvant was demonstrated in vivo in both murine and nonhuman primate models. Taken together, K3-SPG may be useful for immunotherapeutic applications that require type I and type II IFN as well as CTL induction.

innate immunity | two-photon microscopy | MARCO | Siglec-1 | β-glucan

CpG oligodeoxynucleotide (CpG ODN) is a short (~20 bases), single-stranded synthetic DNA fragment containing the immunostimulatory CpG motif, a potent agonist for Toll-like receptor 9 (TLR9), which activates dendritic cells (DCs) and B cells to produce type I interferons (IFNs) and inflammatory cytokines (1, 2) and acts as an adjuvant toward both Th1-type humoral and cellular immune responses, including cytotoxic T-lymphocyte (CTL) responses (3, 4). Therefore, CpG ODN has been postulated as a possible immunotherapeutic agent against infectious diseases, cancer, asthma, and pollinosis (2, 5).

There are at least four types of CpG ODN, each of which has a different backbone, sequence, and immunostimulatory properties (6). D-type (also called A) CpG ODNs typically comprise one palindromic CpG motif with a phosphodiester (PO) backbone and phosphorothioate (PS) poly(G) tail, and activates plasmacytoid DCs (pDCs) to produce a large amount of IFN-α but fails to induce pDC maturation and B-cell activation (7, 8). The three other types of ODN consist of a PS backbone. K-type (also called B) CpG ODN contains nonpalindromic multiple CpG motifs, and strongly activates B cells to produce IL-6 and pDCs to maturation but barely produces IFN-α (8, 9). Recently, C and P CpG ODNs have been developed; these contain one and two palindromic CpG sequences, respectively, both of which can activate B cells like K-type and pDC like D-type, although C

CpG ODN induces weaker IFN-α production compared with P CpG ODN (10–12).

D and P CpG ODNs have been shown to form higher-order structures, Hoogsteen base pairing to form parallel quadruplex structures called G tetrads, and Watson–Crick base pairing between cis- and trans-palindromic portions, respectively, that are required for robust IFN-α production by pDCs (12–14). Although such higher-order structures appear necessary for localization to early endosomes and signaling via TLR9, they suffer from product polymorphisms, aggregation, and precipitation, thereby hampering their clinical application (15). Therefore, only K and C CpG ODNs are generally available as immunotherapeutic agents and vaccine adjuvants for human use (16, 17). Although K CpG ODN enhances the immunogenicity of vaccines targeting infectious diseases and cancers in human clinical trials (6, 17), chemical or physical conjugation between antigen and K CpG ODN is necessary for optimal adjuvant effects. These results indicate that these four (K, D, P, and C) types of CpG ODN have advantages and disadvantages; however, the

Significance

CpG oligodeoxynucleotide (ODN), a Toll-like receptor 9 ligand, is a promising immunotherapeutic agent; however, developing an IFN-inducing CpG ODN forming a stable nanoparticle without aggregation has been unsuccessful. Here we generated a nanoparticulate CpG ODN (K3) wrapped by the nonagonistic Dectin-1 ligand schizophyllan (SPG), K3-SPG. K3-SPG stimulates human peripheral blood mononuclear cells to produce large amounts of both type I and II IFN. K3-SPG thus became a potent adjuvant, especially for cytotoxic T-lymphocyte (CTL) induction to coadministered protein antigens without conjugation, which is attributable to its nanoparticulate nature rather than to targeting Dectin-1. Protective potency of K3-SPG as an influenza vaccine adjuvant was demonstrated in both murine and nonhuman primate models. K3-SPG may be used as an IFN inducer as well as a CTL inducer for immunotherapeutic applications.

—229—

development of an "all-in-one" CpG ODN activating both B cells and pDCs that forms a stable nanoparticle without aggregation has yet to be accomplished. A better strategy, targeting CpG ODN toward antigen-presenting cells (APCs), is desired to improve immunostimulatory specificity and immunotherapeutic efficacy of CpG ODNs.

Schizophyllan (SPG), a soluble β-glucan derived from *Schizophyllum commune*, is a drug that has been approved in Japan as an enhancer of radiotherapy in cervical carcinoma patients for the last three decades (18). It has been shown to form a complex with polydeoxyadenylic acid (dA) as a triple-helical structure (19). Although we previously demonstrated that mouse and humanized CpG ODN with PO poly(dA) at the 5′ end complexed with SPG enhanced cytokine production and acted as an influenza vaccine adjuvant (20, 21), it has been difficult to achieve high yields of the CpG–SPG complex toward its more efficient and cost-effective preclinical as well as clinical development. Recently, when the PS backbone of the dA sequence was linked to CpG ODN, the efficacy of complex formation was elevated by nearly 100% (22). However, a thorough investigation has yet to be conducted to identify the best humanized CpG sequence and optimization of factors to gain all-in-one activities of the four types of CpG ODN.

To do this, we sought to optimize a humanized CpG–SPG complex as a vaccine adjuvant and immunostimulatory agent in humans (in vitro), mice (in vitro and in vivo), and nonhuman primates (in vivo). In this study, we identified a novel K CpG ODN (K3) and SPG complex, namely K3-SPG. It forms a higher-order nanoparticle that can be completely solubilized. We found that this all-in-one K3-SPG displayed a more potent activity than, and different characteristics from, any other type of CpG ODN and previous CpG–SPG complexes.

Results

A Rod-Shaped Nano-Sized Particle of K3-SPG Gains Dual Characteristics of K- and D-Type CpG ODNs.

To make a complex between CpG ODNs and schizophyllan (SPG), CpG ODNs need additional sequences of phosphorothioate backbone of 40-mer polydeoxyadenylic acid (dA_{40}) at the 5′ or 3′ end (20, 22). Fig. 1A shows methods of CpG ODN and SPG complexation through denaturing–renaturing procedures. In this study, we selected K3 as a K-type CpG ODN. At first, we examined the immunostimulatory impacts of the 5′ and 3′ ends of CpG ODN. 5′-K3-dA_{40}-3′, but not 5′-dA_{40}-K3-3′, complexed with SPG-activated human peripheral blood mononuclear cells (PBMCs) to produce a robust amount of IFN-α (Fig. 1B and Fig. S1). K3, K3-dA_{40}, or dA_{40}-K3, which are able to activate human PBMCs to produce other cytokines such as IL-6, failed to produce IFN-α (Fig. 1B and Fig. S1). These results indicate that the 5′-CpG sequence (K3-SPG) is more desirable than the 3′-CpG sequence as a novel TLR9 agonist. Although some CpG ODN-induced cytokine production is known to have a dose-dependent correlation, K3-SPG–induced IFN-α production is not. Given that previous reports showed that IFN-α pro-duction by K CpG ODN stimulation has a bell-shaped dose–response correlation (7), altogether these results suggest that K3-SPG still has the character of K CpG ODN.

Qualification and quantitation of K3-SPG were conducted by scanning electron microscopy (SEM) and dynamic light scattering (DLS). K3-SPG had a rod-like structure, consistent with that seen in a previous report (23) (Fig. 1C). It appeared to be a soluble monomeric nanoparticle with an average diameter of 30 nm, comparable to SPG itself and smaller than D CpG ODN (D35) (14, 24) (Fig. 1D). Given that K3-SPG forms a nanoparticle, we compared the immunostimulatory activities of K3-SPG with D, C, and P CpG ODNs. PBMCs stimulated with K3-SPG produced larger amounts of IFN-α and IFN-γ but at far lower concentrations than those induced by D35 (Fig. 1E) and P and C CpG ODNs (Fig. S2). These results suggest that K3-SPG gains the characteristic of D CpG ODN without losing that of the K type, because these IFNs are known to be D type-specific cytokines (7, 8, 25). To understand the dual functions of K and D
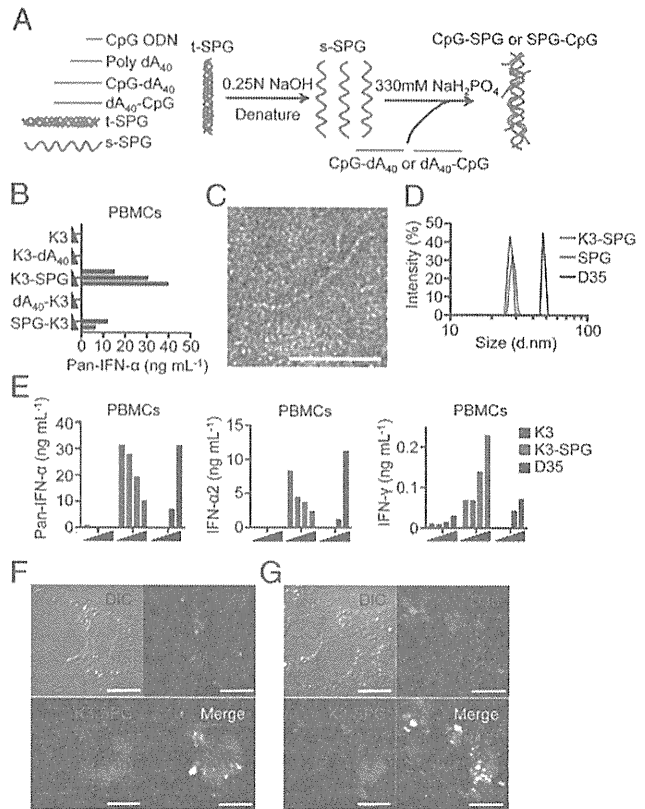

Fig. 1. K (B) CpG ODN and SPG complex forms nanoparticles and gains D (A) CpG ODN characteristics. (A) Methods of CpG ODN and SPG complexation. tSPG, triple-stranded SPG; sSPG, single-stranded SPG. (B) Production of IFN-α by human PBMCs stimulated with K3, K3-dA_{40}, K3-SPG, dA_{40}-K3, or SPG-K3 (adjusted for K3 ODN concentration at 0.1, 0.3, or 1 μM) for 24 h was measured by ELISA. (C) K3-SPG processed for SEM. (Scale bar, 50 μm.) (D) Size of K3-SPG, SPG, and D35 was analyzed by DLS. (E) Production of type I and II IFNs by PBMCs stimulated with K3, K3-SPG, or D35 for 24 h was measured by ELISA. (F and G) Mouse BMDMs were stimulated with Alexa 488-K3 (F) or Alexa 488-D35 (G) and Alexa 647-K3-SPG at 1 μM for 3 h. The cells were incubated with Hoechst 33258, fixed, and analyzed by fluorescence microscopy. DIC, differential interference contrast. (Scale bars, 10 μm.) Data represent one of three independent experiments with similar results.

CpG ODNs, we analyzed the intracellular localization of K3-SPG in bone marrow-derived macrophages (BMDMs). K3-SPG was colocalized with not only the endosomes containing K CpG ODN but also those containing D CpG ODN (Fig. 1 F and G) such as C CpG ODN (26), suggesting that K3-SPG may transduce endosome-mediated innate immune signaling pathways by K and D CpG ODNs. These results strongly suggest that K3-SPG forms a nano-sized higher-order and completely solubilized particle and found that this all-in-one K3-SPG displayed a more potent activity than, and different characteristic from, any other CpG ODNs and previously known CpG–SPG complex.

K3-SPG Is a Prominent Vaccine Adjuvant That Induces Potent CTL Responses to Protein Antigen Without Conjugation.

We compared the adjuvant effects of K3, K3-dA_{40}, and K3-SPG in a murine immunization model. When wild-type mice were immunized with LPS-free chicken ovalbumin protein (OVA) alone or OVA with each K3-derived adjuvant, K3-SPG induced significantly higher humoral immune responses (Fig. 2A) and stronger T-cell responses than that induced by K3 (Fig. 2B). Of note, tetramer assays revealed a significantly greater number of OVA-specific CD8 T cells (Fig. 2C). We also observed very strong in vivo CTL activity against
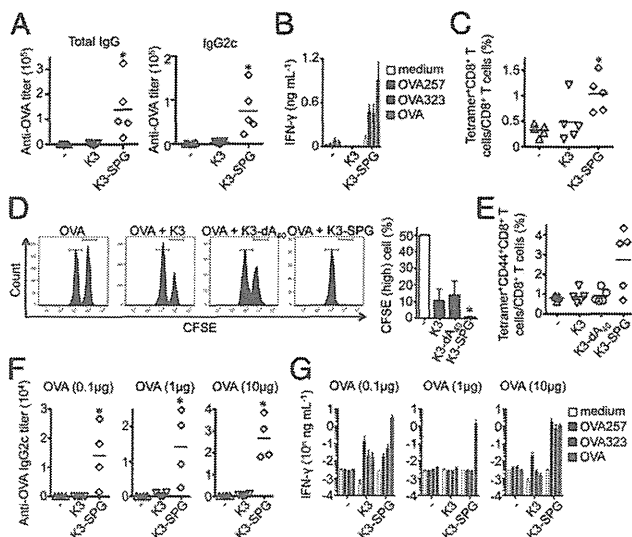
-230-

Fig. 2. K3-SPG acts as a potent vaccine adjuvant by simple mixture with antigen. Adjuvant activities of K3-SPG were analyzed. C57BL/6J mice ($n = 4$ or 5) were immunized s.c. with OVA protein antigen and various adjuvants. OVA-specific serum IgG (A), IFN-γ (B), and OVA$_{257-264}$-specific tetramer (C) were monitored (d17) after immunization (d0 and d10) with OVA (100 μg) with or without K3 (10 μg) or K3-SPG (10 μg). (D) In vivo CTL assay 7 d after priming with OVA and various adjuvants as indicated. (E) Immunization with OVA$_{257-264}$ peptide (10 μg) with or without adjuvant as indicated. (F and G) Dose-sparing study; OVA-specific serum IgG and IFN-γ were monitored after immunization as in A and B. *$P < 0.05$ (Mann–Whitney U test). Data represent one of two or three independent experiments with similar results.

coadministered protein antigens lacking any covalent conjugation (Fig. 2D). This strong CTL induction by K3-SPG was reproduced by peptide vaccination (Fig. 2E) and was dose-dependent (Fig. S3). The antigen-sparing ability of K3-SPG was so potent that comparable antibody and CD4 T-cell responses were achieved using one-hundredth the amount of OVA antigen (Fig. 2 F and G). These results clearly indicate that K3-SPG is a more prominent adjuvant than K3 alone.

SPG Is a Soluble Dectin-1 Ligand but Is Not a Dectin-1 Agonist. We examined the role of Dectin-1 in cellular uptake of, and following activation by, SPG and K3-SPG, as Dectin-1 has been shown to be a receptor for β-glucans such as Zymosan (27). Using flow cytometry, we found that HEK293 cells expressing Dectin-1 but not Dectin-2 or a control (vector) increased the uptake of SPG or K3-SPG in vitro regardless of ODN presence (Fig. 3 A and B). It has recently been reported that the soluble form of β-glucan does not activate Dectin-1 signaling (28). Additionally, Dectin-1 signaling inhibits TLR9-mediated cytokine production through suppressor of cytokine signaling 1 induction (29). Therefore, we examined the agonistic activity of SPG. When splenocytes were stimulated with Zymosan-Depleted but not SPG, dose- and Dectin-1–dependent TNF-α and other cytokine production was observed, whereas cytokine production by Zymosan and Curdlan was Dectin-1–independent (Fig. 3C and Fig. S4). Zymosan-Depleted inhibited CpG ODN-induced IFN-α, with this inhibition relieved by Dectin-1 deficiency (Fig. 3D). In contrast, SPG did not inhibit CpG ODN-induced IFN-α production (Fig. 3E). These results indicate that SPG is a ligand but not an agonist of Dectin-1; therefore, SPG does not interfere with TLR9-mediated IFN-α production.

Adjuvant Effects of K3-SPG Are Dependent on TLR9 and Partially Dependent on Dectin-1. Because K3-SPG is a complex of CpG ODN and β-glucan, we examined the role of TLR9 (1) and Dectin-1 (30) using receptor knockout mice. When splenocytes

and Flt3 ligand-induced bone marrow-derived DCs (FL-DCs) from *Tlr9-* and *Dectin-1–*deficient mice were stimulated with K3-SPG, cytokine production was completely dependent on TLR9 but not Dectin-1, excluding IL-12 p40 production (Fig. 4 A–D). K3-SPG–induced IL-12 p40 production showed two peaks, where the first peak of its production, but not the second peak at a higher dose, was dependent on Dectin-1 (Fig. 4D). This result may imply that Dectin-1 expression is involved in IL-12 p40 production at a lower dose of K3-SPG in vitro. Consistent with in vitro results, immunization of *Tlr9-*deficient mice with K3-SPG plus OVA resulted in diminished humoral and T-cell responses (Fig. 4 E–G). *Dectin-1–*deficient mice showed comparable immune responses with wild-type mice when the mice were immunized with OVA plus 10 μg of K3-SPG (Fig. S5). When *Dectin-1–*deficient mice were immunized with OVA plus 1 μg of K3-SPG, mice exhibited a reduced CD8 T-cell response according to the tetramer assays (Fig. 4J), with no significant changes in antibody and cytokine production from T cells (Fig. 4 H and I). These results suggest that the adjuvant effect of K3-SPG is dependent on TLR9 signaling. Although SPG and K3-SPG do not stimulate Dectin-1 signaling, the effect of K3-SPG is still partially dependent on Dectin-1 in vivo.

MARCO⁺, but Not Siglec-1⁺, Macrophages in Draining Lymph Nodes Dominantly Capture K3-SPG with Antigen. Given that K3-SPG provides potent adjuvant effects in vivo through immunization with a simple antigen mixture, we hypothesized that cells that capture both antigen and K3-SPG should play a critical role in mediating adjuvant effects. To examine in vivo distribution of fluorescence-labeled OVA and K3-SPG, we used fluorescence microscopy and two-photon microscopy. After an injection at the
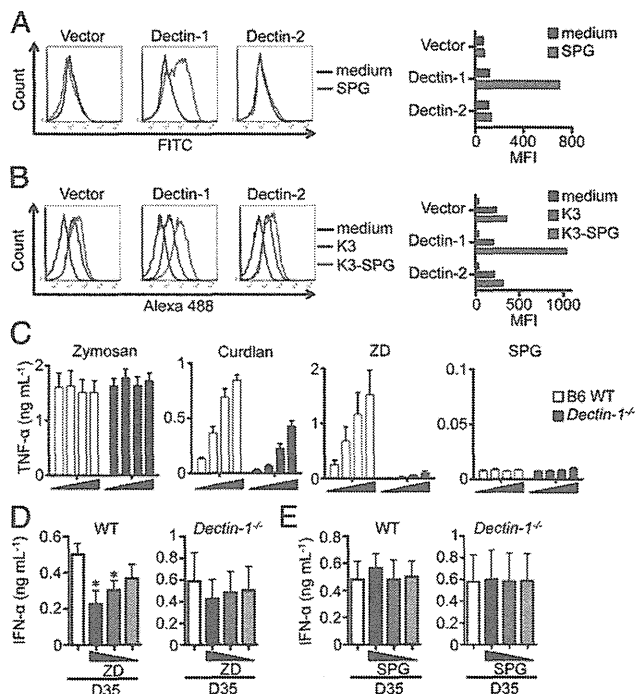

Fig. 3. SPG is a nonagonistic Dectin-1 ligand, but does not interfere with TLR9-mediated IFN-α production. (A and B) HEK293 cells transiently expressing Dectin-1 or Dectin-2 were treated with SPG-FITC (A), Alexa 488-K3, or Alexa 488-K3-SPG (B) for 60 min, and then their cellular uptake was monitored by flow cytometry [Left, histogram; Right, mean fluorescent intensity (MFI)]. Splenocytes from C57BL/6J and *Dectin-1⁻/⁻* mice ($n = 3$) were stimulated with Zymosan, Curdlan, Zymosan-Depleted (ZD), or SPG (3.7–100 μg/mL) (C), with D35 (1 μM), or with or without ZD (11.1–100 μg/mL) (D) or SPG (E) for 24 h and supernatant cytokines were monitored by ELISA. *$P < 0.05$ (t test). Data represent one of three independent experiments with similar results.
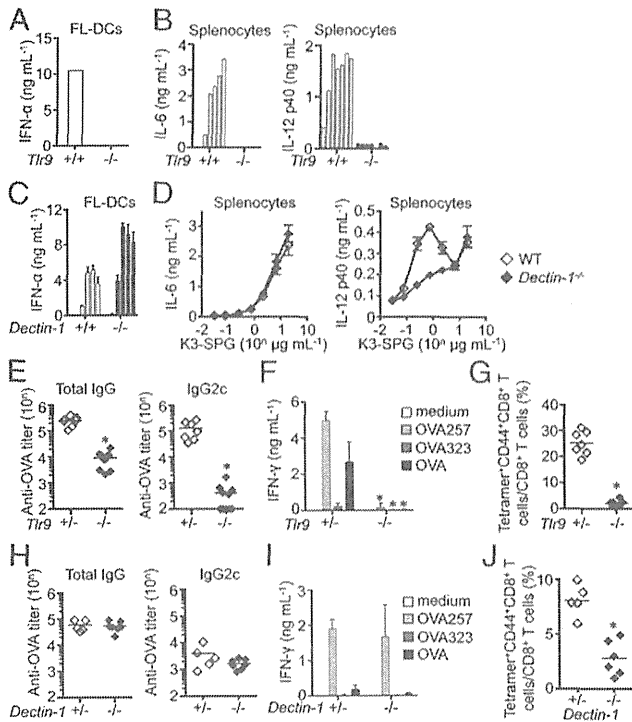
–231–

Fig. 4. Adjuvant effects of K3-SPG were completely dependent on TLR9 and partially on Dectin-1. FL-DCs (A and C) or splenocytes (B and D) from C57BL/6J, $Tlr9^{-/-}$, or $Dectin$-$1^{-/-}$ mice were stimulated with K3-SPG [20 μg/mL (A), 0.014–10 μg/mL (B), or 0.014–10 μg/mL (C and D)] for 24 h, and their cytokine production was monitored by ELISA. $Tlr9^{+/-}$ ($n = 7$) or $Tlr9^{-/-}$ mice ($n = 10$) (E–G) and $Dectin$-$1^{+/-}$ ($n = 5$) or $Dectin$-$1^{-/-}$ mice ($n = 6$) (H–J) were immunized s.c. with OVA (100 μg) and K3-SPG [10 μg (E–G) or 1 μg (H–J)] at days 0 and 10. Seven days after the last immunization, OVA-specific serum IgG (E and H), IFN-γ (F and J), and $OVA_{257-264}$-specific tetramer (G and J) were monitored. $*P < 0.05$ (Mann–Whitney U test). Data represent one of two or three independent experiments with similar results.

base of the tail, both antigen and adjuvant reached the surface of draining inguinal lymph nodes (iLNs) within 1 h (Fig. 5 A, B, and D). After 24 h, some K3-SPG had moved to the $CD3e^+$ T-cell area and colocalized with DQ-OVA (Fig. S6A). Those cells that contained both K3-SPG and DQ-OVA in the T-cell area of the iLNs were $CD11c^+$ DCs (Fig. S6B).

Of interest, the majority of fluorescence signals remained on the surface of the iLNs (Fig. 5A), prompting us to focus on two types of macrophages known to be distributed on the LN surface, Siglec-1$^+$ (also called CD169 or MOMA-1) macrophages (also known as subcapsular sinus macrophages) and MARCO$^+$ macrophages (31). Histological analysis using conventional fluorescence microscopy did not suitably reveal the entire iLN surface; moreover, these macrophages were difficult to isolate for flow cytometric analysis (32, 33). Hence, we used two-photon microscopy imaging analysis to clarify the distribution of antigen and K3-SPG ex vivo. After the injection of anti-MARCO and –Siglec-1 antibodies, specific macrophages were visualized (Movie S1). When the iLN surface was monitored by two-photon microscopy at 1 h postinjection, OVA and K3-SPG were colocalized with MARCO$^+$ but not Siglec-1$^+$ macrophages (Fig. 5 B and D, Fig. S7 A–D, and Movies 2–5). Previous reports suggest that the immune complex and inactivated influenza virus are captured by Siglec-1$^+$ macrophages to induce humoral immune responses (34, 35). The distribution pattern perfectly matched that for MARCO$^+$ macrophages in the iLNs and did not colocalize with Siglec-1$^+$ macrophages, as confirmed by Volocity's colocalization analysis (Perkin Elmer) (Fig. 5 B–E). In contrast, K3 was more

diffusely distributed between MARCO$^+$ and Siglec-1$^+$ areas compared with K3-SPG (Fig. 5 D and E, Fig. S7 C–E, and Movies 6 and 7). Additionally, both $Tlr9$- and $Dectin$-1-deficient mice showed comparable localization of K3-SPG (Fig. S7 F and G).

To determine the contribution of these macrophages toward the adjuvant effects of K3-SPG, we examined different recovery kinetics of macrophages and DCs following an injection of clodronate liposomes into the base of the tail. After the injection, the macrophages were completely depleted by day 2. These cells did not recover for at least 1 wk, whereas DCs were mostly recovered by day 7, as previously reported (36). When both macrophages and DCs were depleted, immune responses were significantly suppressed [Fig. 5F, Clo (−d2)]. When only macrophages, but not DCs, were depleted, the immune responses were comparable to those in untreated mice [Fig. 5F, Clo (−d7)]. This would suggest that although both OVA and K3-SPG were mainly captured by
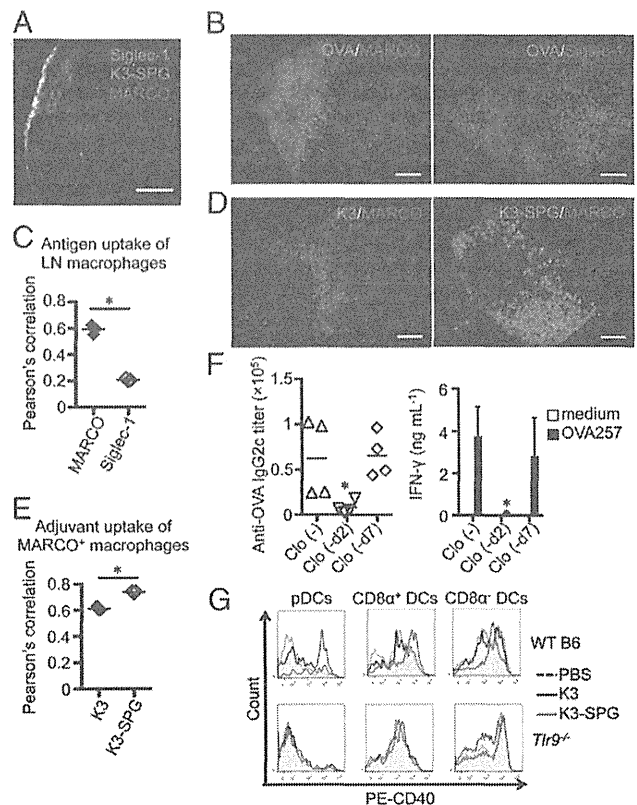

Fig. 5. Role of lymph node macrophages and dendritic cells in uptake and adjuvant effects of K3-SPG. (A) Immunohistochemistry of mouse inguinal LNs after Alexa 488-K3-SPG injection. One hour after injection, the LNs were collected and stained with anti-MARCO-phycoerythrin (PE) and anti–Siglec-1-APC antibodies. (B–E) Two-photon microscopic analysis of LNs. DQ-OVA, Alexa 488-K3, or Alexa 488-K3-SPG was injected as indicated, and anti–MARCO-PE or anti–Siglec-1-PE antibodies were administered. The LNs were collected 1 h later and analyzed by two-photon microscopy. (C and E) Colocalization of antigen or adjuvant with the stained macrophages was analyzed by Pearson's correlation. (F) Clodronate liposomes were injected into C57BL/6J mice either 2 or 7 d before immunization ($n = 4$). Mice were administered OVA (100 μg) plus K3-SPG (10 μg) at day 0. Eight days after immunization, OVA-specific serum IgG and IFN-γ were monitored. (G) C57BL/6J and $Tlr9^{-/-}$ mice were administered s.c. with K3 (10 μg) or K3-SPG (10 μg). At 24 h postadministration, the LNs were collected and the prepared cells were stained and analyzed by flow cytometry. (Scale bars, 100 μm.) $*P < 0.05$ (t test or Mann–Whitney U test). Data represent one of two or three independent experiments with similar results.

Kobiyama et al.

MARCO$^+$ macrophages in the LNs after injection, the macrophages were dispensable to inducing adaptive immune responses. In other words, the adjuvant effect of K3-SPG was largely dependent on the DC population.

K3-SPG Targets and Strongly Activates the Antigen-Bearing DC Population in Vivo.
Our findings suggest that although a large portion of nanoparticulate K3-SPG was taken up by MARCO$^+$ macrophages in iLNs after injection, the adjuvant effects appear to be controlled by DCs. We focused on antigen and adjuvant uptake by the DC population in iLNs. At 24 h postinjection, the uptake of antigen and adjuvants by the DC population was analyzed by flow cytometry. The frequency of CpG-positives in three DC subsets (pDCs, CD8α$^+$ DCs, and CD8α$^-$ DCs) was significantly increased after K3-SPG injection than with K3 (Fig. S8A). In contrast, the frequency of OVA-positive DCs was comparable after K3 and K3-SPG injections (Fig. S8B). When we focused on both antigen- and adjuvant-positive DCs, there was a substantial increase for K3-SPG over K3 (Fig. S9). Both pDCs and CD8α$^+$ DCs in iLNs were strongly activated by K3-SPG but not by K3 24 h postinjection, and this was completely dependent on TLR9 (Fig. 5G). Our results indicate that pDCs and CD8α$^+$ DCs preferentially capture nanoparticulate K3-SPG rather than nonparticulate K3 for maturation and to exert adjuvant effects.

K3-SPG Is a Potent Adjuvant for Influenza Vaccine in Murine and Nonhuman Primate Models.
Finally, we sought the adjuvant effect of K3-SPG by using more clinically relevant influenza vaccination models in both mice and nonhuman primates. When mice were immunized with ether-treated hemagglutinin antigen-enriched virion-free split vaccine (SV) plus the indicated adjuvant, K3-SPG demonstrated superior adjuvant effects to K3 when antibody responses (Fig. S10A) and T-cell responses (Fig. S10B) were compared. More importantly, SV plus K3-SPG immunization resulted in a 100-fold greater antibody response, even compared with vaccination using a whole (virion) inactivated vaccine (WIV) (0.2 μg per mouse) (Fig. 6A), which contains viral RNA as a built-in adjuvant (21). Interestingly, SV (0.1 μg per mouse) plus K3-SPG strongly induced both CD8 and CD4 T-cell responses (Fig. 6B). Mice immunized with SV and K3-SPG exhibited less body weight loss than WIV-immunized mice (Fig. 6C). Strikingly, K3-SPG conferred 100% protection against lethal PR8 virus challenge at the dose of which only 10% of WIV-vaccinated mice survived (Fig. 6D). These results strongly support the notion that K3-SPG works as a potent adjuvant for protein or protein-based vaccines in a murine model, prompting us to extend this finding to a nonhuman primate model using the cynomolgus monkey (*Macaca fascicularis*). Each group of three cynomolgus monkeys was immunized with SV plus K3 or K3-SPG at days 0 and 14. Serum antibody titers were then monitored for 8 wk. The SV plus K3-SPG induced significantly higher antibody titer at 2 wk postimmunization, and titer levels remained high for at least another 6 wk (Fig. 6E). Although antibody titers were reduced at 110 wk after immunization, the K3-SPG group had higher antibody titers than the K3 group (Fig. 6E). When PBMCs were stimulated with SV and WIV, IFN-γ was detected from the SV plus K3-SPG–immunized group (Fig. 6F). Taken together, these results suggest that K3-SPG is a prominent vaccine adjuvant in a nonhuman primate model.

Discussion
The medical need for novel, potent, and safe adjuvants is ever-increasing these days as (*i*) recombinant vaccine antigens such as proteins and peptides are short on natural adjuvants, unlike attenuated or inactivated whole microbial antigens, (*ii*) conventional aluminum salts and oil adjuvants are limited or preferred for enhancing humoral immune responses, and (*iii*) new adjuvants that can induce cellular immune responses, including CTLs, are needed, for example for cancer vaccines. The last two decades have resulted in tremendous progress with respect to adjuvant research and development. A hallmark of the new gen-
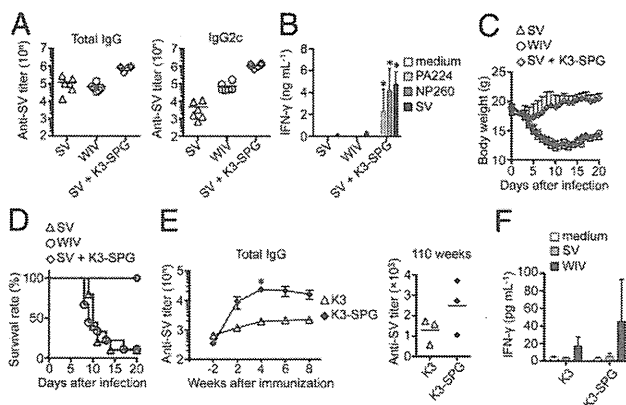

Fig. 6. K3-SPG acts as an influenza vaccine adjuvant in mice and nonhuman primates. (*A–D*) C57BL/6J mice (*n* = 6 or 10) were immunized with SV (0.1 μg), whole inactivated vaccine (WIV) (0.2 μg), or SV (0.1 μg) plus K3-SPG (10 μg) at days 0 and 14. Seven days after the final immunization, SV-specific serum IgG titers (*A*) and IFN-γ (*B*) [specific to SV antigen, PA$_{224-233}$ (PA224) (10 μg/mL) or NP$_{260-283}$ (NP260)] were monitored. (*C* and *D*) Fourteen days after the final immunization, mice were challenged with a 10-LD$_{50}$ dose of influenza virus A/PR/8 (H1N1). Changes in body weights (*C*) and mortality (*D*) were monitored for the next 20 d. (*E* and *F*) Cynomolgus monkeys (*n* = 3) were immunized with SV (5 μg) plus K3 (5 nmol) or SV plus K3-SPG (5 nmol) at days 0 and 14. (*E*) Serum samples were collected at −2, 2, 4, 6, 8, and 110 wk. Antigen-specific serum antibody titers were measured by ELISA. (*F*) PBMCs were prepared from individual cynomolgus monkey blood at 4 wk after the first immunization and restimulated in vitro with medium, SV (10 μg), or WIV for 24 h. Mouse IFN-γ in the supernatants was determined by ELISA. *P < 0.05 (*t* test or Mann–Whitney U test).

eration of adjuvants is that nucleic acids have been rediscovered to be immunologically active in stimulating specific innate immune receptors of the host, in particular TLRs. CpG DNA, a ligand for TLR9, is one of the most promising immunotherapeutic agents that has been identified.

Although there are several types of potent humanized CpG ODN—K (also called B), D (A), C, and P types—the development of an all-in-one CpG ODN activating both B cells and pDCs to form a stable nanoparticle without aggregation has been less than successful. In this study, we generated a novel K CpG ODN that we designated K3-SPG. Although it had been reported that there are molecular interactions between single-stranded nucleic acids and β-glucan (37) and that murine and humanized CpG ODNs can be wrapped by SPG to increase their original TLR9-agonistic activities (20), our report demonstrates that a rod-shaped nano-sized K3-SPG particle exhibits dual characteristics of K and D CpG ODNs (Fig. 1). K3-SPG is distinct from other previously reported K CpG ODNs, including K3. In turn, K3-SPG becomes a D CpG ODN, stimulating human PBMCs to produce large amounts of both type I and type II IFN, targeting the same endosome where the IFN-inducing D type resides without losing its K-type activity (Fig. 1 *F* and *G*). Another surprising finding is that this K3-SPG forms a rod-like single nanomolecule (Fig. 1 *C* and *D*). This is advantageous over previously demonstrated D or P types, whose ends form higher-order structures that may hamper further development as prodrugs, including good manufacturing practice assignment.

Another prominent feature of this K3-SPG is its potency as an adjuvant for induction of both humoral and cellular immune responses, especially CTL induction, to coadministered protein antigens without conjugation. Such potent adjuvant activity of K3-SPG is attributable to its nanoparticulate nature (Figs. 1 *C* and *D* and 2) rather than targeting Dectin-1 by SPG (Figs. 3 and 4). Initially, we hypothesized that K3-SPG becomes such a potent adjuvant because it targets Dectin-1, because SPG is a β-1,3-glucan, and seems to be a clear Dectin-1 ligand (Fig. 3A). Our other results, however, led us to conclude that the role of Dectin-1